

Mineral assemblages and phase equilibria of metabasites from the prehnite–pumpellyite to amphibolite facies, with the Flin Flon Greenstone Belt (Manitoba) as a type example

Paul G. Starr¹  | David R. M. Pattison¹  | Doreen E. Ames²

¹Department of Geoscience, University of Calgary, Calgary, AB, Canada

²Geological Survey of Canada, Ottawa, ON, Canada

Correspondence

Paul G. Starr, Department of Geoscience, University of Calgary, 2500 University Drive NW, Calgary AB T2N 1N4, Canada.
Email: starrp@bc.edu

Present address

Paul G. Starr, Department of Earth and Environmental Sciences, Boston College, 140 Commonwealth Avenue, Chestnut Hill, MA, USA

Funding information

Natural Sciences and Engineering Research Council of Canada, Grant/Award Number: 037233

Handling Editor: Richard White

Abstract

An exceptionally well-exposed part of the Flin Flon Greenstone Belt (Manitoba/Saskatchewan) is used to characterize the mineral assemblage evolution associated with prehnite–pumpellyite through amphibolite facies metamorphism of basalts. Data from these rocks are combined with a large literature data set to assess the ability of current thermodynamic models to reproduce natural patterns, evaluate the use of metabasic rocks at these grades to estimate pressure–temperature (P – T) conditions of metamorphism, and to comment on the metamorphic devolatilization that occurs. At Flin Flon, five major isograds (actinolite-in, prehnite- and pumpellyite-out, hornblende-in, oligoclase-in, and actinolite-out) collectively represent passage from prehnite–pumpellyite to lower amphibolite facies conditions. The evolution in mineral assemblages occurs in two narrow (~1,000 m) zones: the prehnite–pumpellyite to greenschist facies (PP-GS) transition and greenschist to amphibolite facies (GS-AM) transition. Across the GS-AM transition, significant increases in the hornblende and oligoclase proportions occur at the expense of actinolite, albite, chlorite, and titanite, whereas there is little change in the proportions of epidote. The majority of this mineral transformation occurs above the oligoclase-in isograd within the hornblende–actinolite–oligoclase zone. Comparison with thermodynamic modelling results suggests data set 5 (DS5) of Holland and Powell (1998, *Journal of Metamorphic Geology*, **16**(3):309–343) and associated activity–composition (a – x) models is generally successful in reproducing natural observations, whereas data set 6 (DS6) (Holland & Powell, 2011, *Journal of Metamorphic Geology*, **29**(3):333–383) and associated a – x models fail to reproduce the observed mineral isograds and compositions. When the data from Flin Flon are combined with data from the literature, two main pressure-sensitive facies series for metabasites are revealed, based on prograde passage below or above a hornblende–albite bathograd at ~3.3 kbar: a low-pressure ‘actinolite–oligoclase type’ facies series, characterized by the appearance of oligoclase before hornblende, and a moderate- to high-pressure ‘hornblende–albite type’ facies series, characterized by the appearance of hornblende before oligoclase. Concerning the PP-GS transition, the mineral assemblage evolution in Flin Flon suggests it occurs over a small zone (<1,000 m), in which assemblages containing true transitional assemblages (prehnite and/or pumpellyite coexisting with actinolite) are

rare. This contrasts with thermodynamic modelling, using either DS5 or DS6, which predicts a wide PP-GS transition involving the progressive appearance of epidote and actinolite and disappearance of pumpellyite and prehnite. Patterns of mineral assemblages and thermodynamic modelling suggest a useful bathograd ('CHEPPAQ bathograd'), separating prehnite–pumpellyite-bearing assemblages at low pressures and pumpellyite–actinolite-bearing assemblages at higher pressures, occurs at ~2.3 to 2.6 kbar. Observations from the Flin Flon sequence suggests devolatilization across the GS-AM transition (average: ~1.8 wt% H₂O) occurs over a very narrow interval within the actinolite–hornblende–oligoclase zone, associated with the loss of >75% of the total chlorite. By contrast, modelling of the GS-AM transition zone predicts more progressive dehydration of ~2 wt% H₂O over a >50°C interval. Observations from the field suggest devolatilization across the PP-GS transition occurs over a very narrow interval given the rarity of transitional assemblages. Modelling suggests fluid release of 1.0–1.4 wt% resulting from prehnite breakdown over a ~10°C interval. This fluid may not be entirely lost from the rock package due to involvement in the hydration of igneous mineralogy across the PP-GS transition as observed in the Flin Flon sequence.

KEYWORDS

amphibolite facies, greenschist facies, greenstone belt, metamorphic devolatilization, prehnite–pumpellyite facies

1 | INTRODUCTION

Metamorphosed basalts spanning the prehnite–pumpellyite to amphibolite facies represent some of the most abundant metamorphic rocks on the planet, forming a component of most orogenic belts and representing the dominant metamorphic lithology within Archaean and Proterozoic greenstone belts (e.g. Furnes, Dilek, & De Wit, 2015). Understanding the metamorphic evolution of such rocks is needed to constrain the thermal regime that existed during metamorphism, which in turn provides important insights into the construction of cratonic belts and the geochemical and tectonic evolution of greenstone belts (e.g. Archibald, Bettenay, Binns, Groves, & Gunthorpe, 1978; Furnes et al., 2015). In addition, rocks of this grade within greenstone belts commonly host a variety of ore deposits, including volcanogenic massive sulphide deposits, and the fluids produced as a result of metamorphic devolatilization across the greenschist–amphibolite facies transition have been linked to the formation of orogenic gold deposits (e.g. Elmer, White, & Powell, 2006; Goldfarb et al., 2005; Goldfarb & Groves, 2015; Powell, Will, & Phillips, 1991; Tomkins, 2010, 2013).

Despite their importance, our knowledge of the evolution of metamorphic mineral assemblages in subgreenschist to lower amphibolite facies metabasaltic rocks, and our ability to thermodynamically model these sequences, is more limited

and less explored than for their metapelitic counterparts. In addition, although metapelitic rocks are useful for estimating pressure and temperature (P – T) conditions in rocks of the amphibolite facies and higher (e.g. Carmichael, 1978; Pattison, 2001; Spear & Cheney, 1989), they are of more limited use below the lower amphibolite facies because they show few mineralogical changes. The result has been a limited number of meaningful estimates of the P – T conditions for both metapelitic and metabasic rocks metamorphosed at these grades.

This study aims to improve on our understanding of the metamorphism of basalts from prehnite–pumpellyite to amphibolite facies through the detailed petrological study combined with phase equilibria modelling of a metamorphic sequence within the Flin Flon Greenstone Belt of central Canada (Figure 1). Augmented with observations from a large database of metabasite sequences from the literature, we use the observations from the Flin Flon sequence for a global assessment of the use of metabasic rocks at these grades to estimate P – T conditions and test the ability of thermodynamic modelling techniques to generate phase equilibria consistent with the natural observations. In addition, this data set is used to evaluate the amounts and intervals of metamorphic devolatilization occurring across the key facies transitions within these rocks. The Flin Flon sequence is perhaps the best exposed sequence of its kind in the world and is thus an ideal natural laboratory for this purpose.

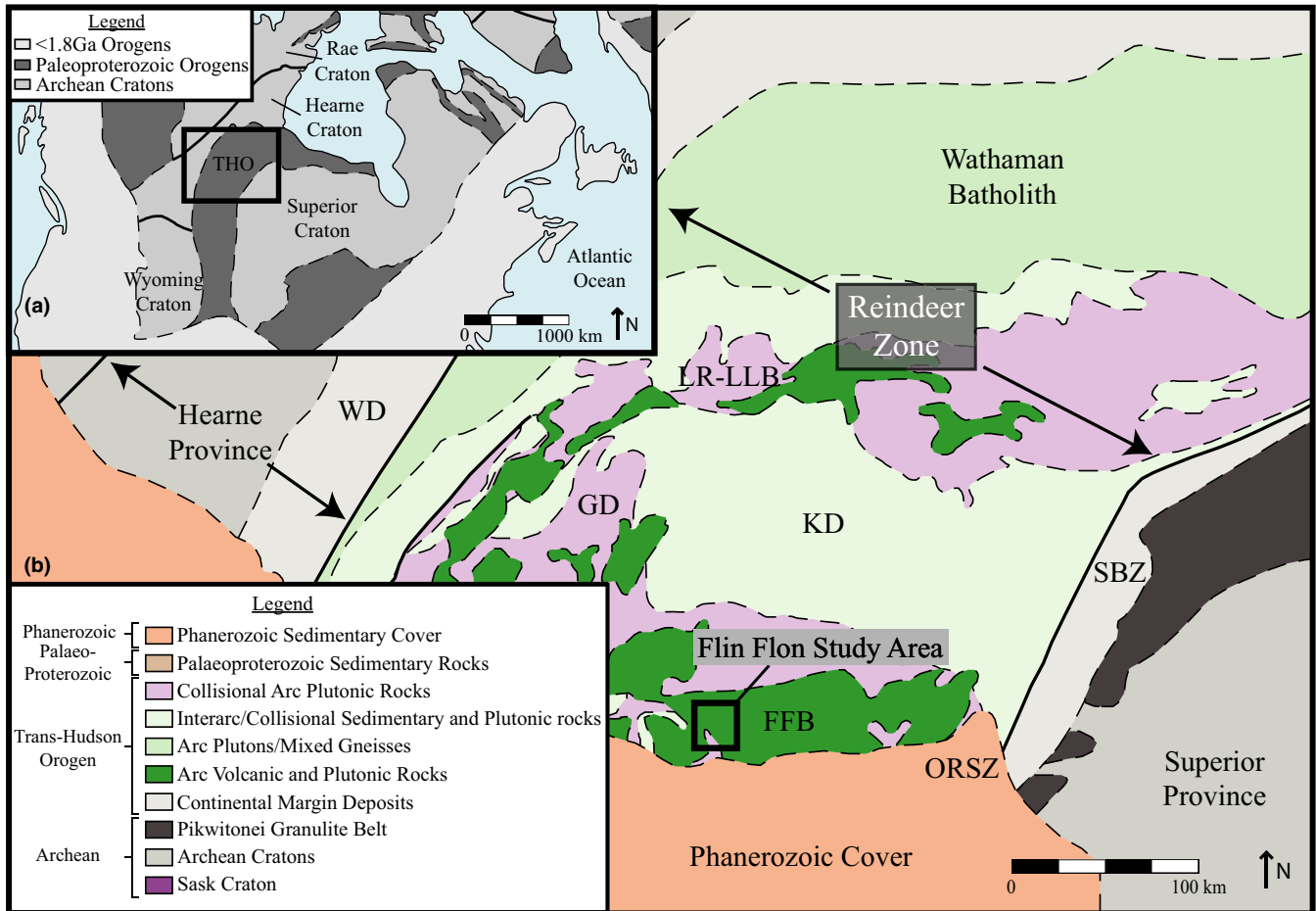


FIGURE 1 (a) Simplified geological map of North America showing the major cratonic and orogenic belts. THO: Trans-Hudson Orogen. Modified after Hoffman (1988) and Lucas et al. (1996). (b) Simplified geology map of the Saskatchewan/Manitoba segment of the Trans-Hudson Orogen. FFB: Flin Flon belt; GD: Glennie Domain; LR-LLB: La Ronge–Lynn Lake Belt; KD: Kiseynew Domain; WD: Wollaston Domain; SPZ: Superior Boundary Zone. Modified after Lucas et al. (1996)

The aims of this study include: (a) detailing the textural, modal, and compositional changes across the prehnite–pumpellyite–greenschist facies (PP-GS) and greenschist–amphibolite facies (GS-AM) transitions in the Flin Flon sequence, in order to constrain the key reactions that take place in these transitions; (b) testing the ability of the latest thermodynamic data sets and $a-x$ relations for metabasites (data set 5.5 of Holland & Powell, 1998, and data set 6.2 of Holland & Powell, 2011, with respective $a-x$ models detailed below) to reproduce the mineral assemblages, mineral compositions, and reactions within the Flin Flon sequence and others from the literature; (c) constraining the $P-T$ conditions of key mineral assemblage changes across the prehnite–pumpellyite to greenschist, and greenschist to amphibolite facies, transitions; (d) identifying pressure-sensitive ‘bathozones’ that separate lower pressure and higher pressure metabasite facies series (mineral assemblage sequences) in metabasites over this range of grade; and (e) characterizing the nature of metamorphic devolatilization across the prehnite–pumpellyite to greenschist, and greenschist to amphibolite facies, transitions.

2 | GEOLOGICAL BACKGROUND

The Flin Flon–Glennie complex (FFGC) forms an elongate E–W-oriented belt, ~250 km in length, traversed by the Saskatchewan–Manitoba border (Figure 1). The FFGC comprises a series of accreted tectono-stratigraphic assemblages that were amalgamated during the Palaeoproterozoic in the early stages of the Trans-Hudson Orogen (THO) (Ansdell, 2005; Lucas, Stern, Syme, & Thomas, 1996; Stauffer, 1984). The area around the townsite of Flin Flon, which forms the main area of interest for this study, is host to a number of current or previously producing Cu–Zn VMS mines (e.g. Flin Flon, Callinan and 777 deposits) (Ames, Galley, Kjarsgaard, Tardif, & Taylor, 2016) and as a result, has been the focus of a large number of studies particularly focusing on the structural and tectonic development of the area (e.g. Bailes & Syme, 1989; Gale, Lucas, & Dixon, 1999; Lafrance et al., 2016).

The majority of the field area (~120 km²) is made up of volcanic rocks comprising the Flin Flon arc assemblage, interpreted to be of island-arc to back-arc affinity (e.g. Syme, Lucas,

Bailes, & Stern, 1999). The Flin Flon arc assemblage may be divided into the Flin Flon, Hidden, and Louis formations, consisting predominantly of basaltic and basaltic andesite volcanic flows and intrusives, rhyolite flows and volcanoclastic rocks (DeWolfe, Gibson, & Piercey, 2009). The Flin Flon formation hosts the Flin Flon, 777 and Callinan VMS deposits (Devine et al., 2002). The Hidden and Louis formations form part of the overlying hangingwall sequence to the ore deposits and are interpreted to be the product of a composite volcanic system predominantly composed of pillowed aphyric or plagioclase phyric basalt/basaltic andesite and mafic volcanoclastics (DeWolfe et al., 2009). The Hidden and Louis formations are unconformably overlain by the fluvial sedimentary Missi group, consisting of deformed conglomerate, sandstone, and siltstone.

3 | METAMORPHIC ISOGRAD MAP

A suite of over 600 thin sections from across the field area was used for this study, complemented by the sample suites used in Digel and Ghent (1994). Figure 2 shows a simplified metamorphic isograd map for the field area. The metamorphic assemblages indicate that the regional metamorphic grade ranges from prehnite–pumpellyite facies in the southeastern portion of the field area to lower amphibolite facies in the northwest where the basaltic sequence is capped by the Missi group sediments. Five regional metamorphic isograds were identified, from south to north: actinolite-in, prehnite- and pumpellyite-out, hornblende-in, oligoclase-in, and actinolite-out. The prehnite-out and pumpellyite-out isograds are coincident within the resolution of the sampling (Figures 2 and 3), and are thus treated as a single isograd. The area consists of two intact sequences that are not disrupted by deformation features, one containing the prehnite–pumpellyite to greenschist transition in the south of the area (Hook Lake Block; Figure 3a) and the other, the greenschist–amphibolite transition in the northern portion of the field area (Flin Flon Block; Figure 3b). These two blocks are separated by post-metamorphic brittle faults such as the Ross Lake and Cliff Lake faults.

The metamorphism in the area post-dates the majority of deformation and foliation development as evidenced by the random orientation of metamorphic minerals in most samples and the lack of deformation of the isograds. The only major post-metamorphic deformation is related to movement along the late NNW-SSE-oriented faults, which affect only a relatively small portion of the field area. These faults include the Ross Lake fault which, as discussed above, results

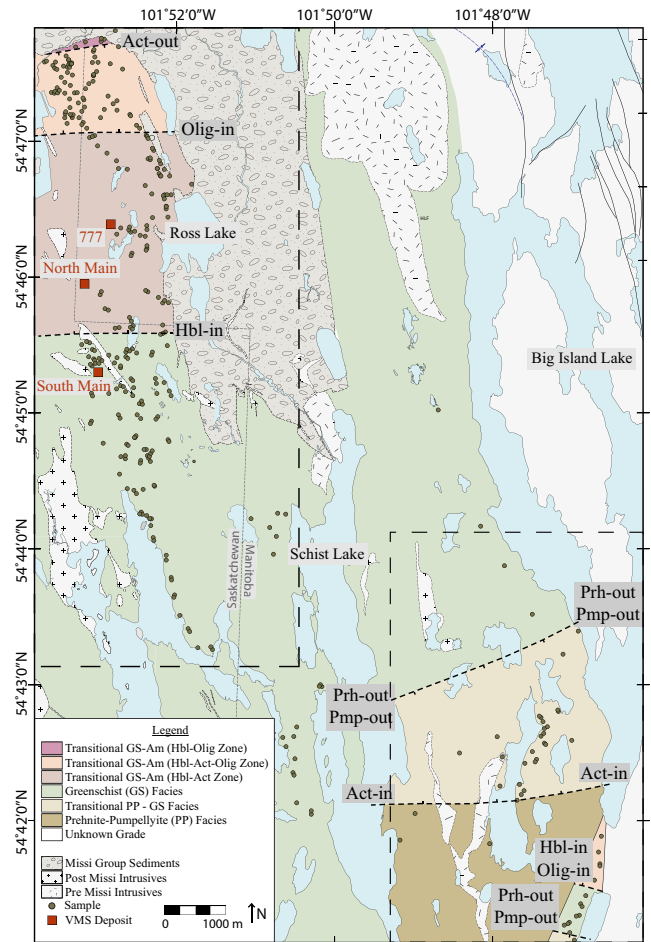


FIGURE 2 Regional metamorphic isograds superimposed on a simplified geology map. Underlying geology based on the maps of Bailes and Syme (1989), Kremer and Simard (2007); and Simard et al. (2010). Sample sites with full mineral assemblage shown by brown dots

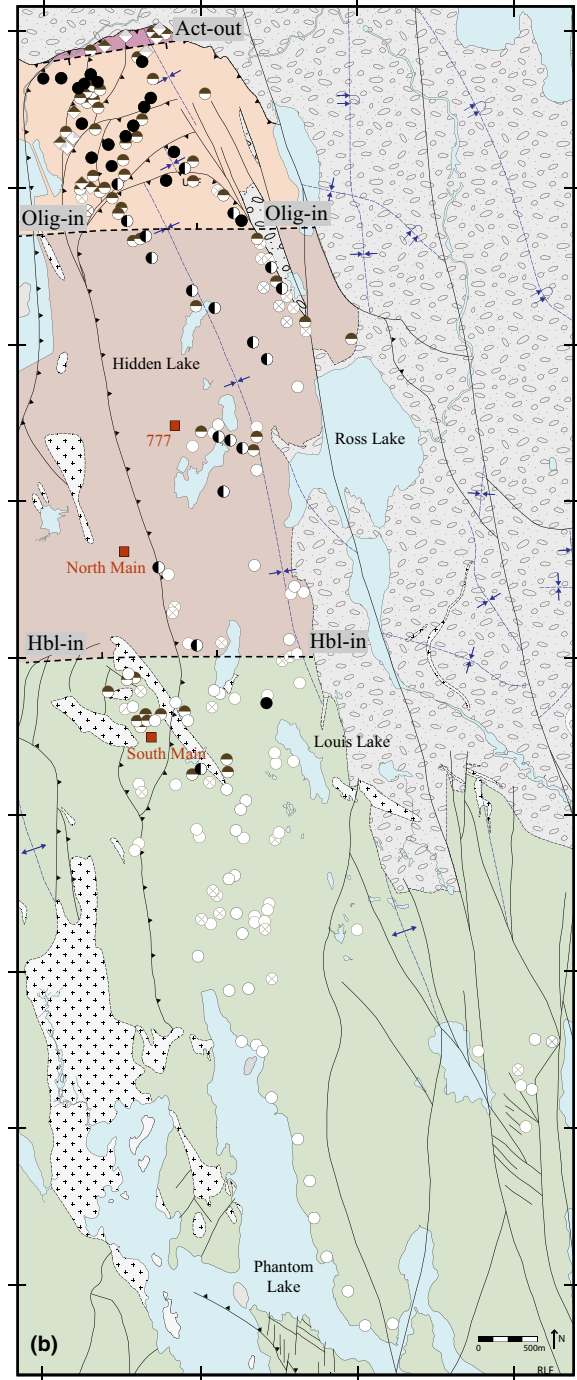
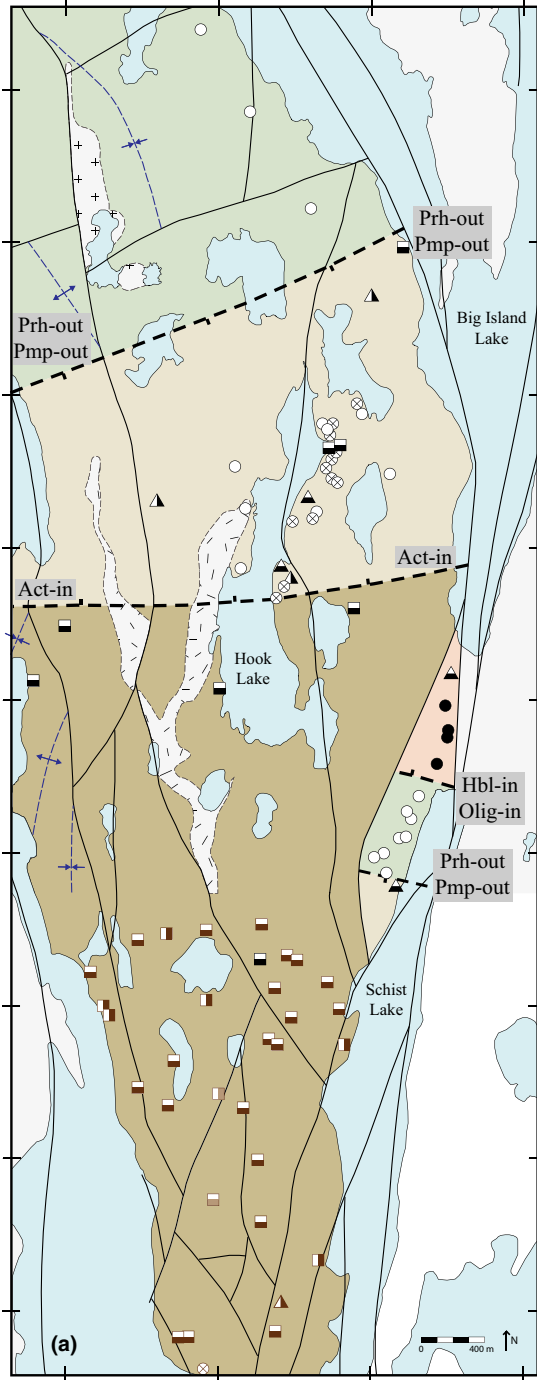
in the separation of the metamorphic sequence into two intact blocks, and the juxtaposition of prehnite–pumpellyite facies rocks against greenschist facies rocks within the southern portion of the field area (Figure 2).

4 | MINERAL ASSEMBLAGES AND TEXTURES

4.1 | Prehnite–pumpellyite facies

The prehnite–pumpellyite facies is characterized by the diagnostic assemblage $Prh + Pmp + Ab + Chl + Ep + Qtz \pm Ttn \pm Cc \pm Ms \pm Kfs \pm Ap$ (mineral abbreviations after Kretz, 1983). Prehnite and pumpellyite coexist in 75% of samples, with the

FIGURE 3 (a) Mineral assemblage map for the southern portion of the Hook Lake block, containing the prehnite–pumpellyite facies to greenschist facies transition. (b) Mineral assemblage map for the Flin Flon block, containing the transition zone from greenschist facies to amphibolite facies. Mineral assemblages with a black rim or infill represent those documented using data from EDS and/or WDS analyses. Mineral assemblages indicated with a brown rim or infill are those determined by petrographic microscope only



Metamorphic mineral assemblages

- | | | | | |
|---------------------|---------------------------|------------------------------------|-------------------------------|--------------------------|
| ○ Ab+Chl | ▲ Act+Prh+Ep+Ab+Chl | +Act | ◇ Hbl+Olig+Ab+Ep+Chl | ----- -Act |
| ⊗ Ab+Chl+Ep | ▲ Act+Pmp+Ep+Ab+Chl | Transitional Prh + Pmp / GS Facies | ◇ Hbl+Olig+Ab+Chl | ----- -Ep |
| ▣ Prh+Ab+Chl | ▲ Act+Prh+Pmp+Ep+Ab+Chl | Greenschist Facies -Prh -Pmp +Hbl | ◇ Hbl+Olig+Ab+Ep | ----- -Chl |
| ▣ Pmp+Ab+Chl | ○ Act+Ab+Ep+Chl | Transitional GS / Amp Facies +Olig | ◇ Hbl+Olig+Ab | ----- Amphibolite Facies |
| ▣ Prh+Pmp+Ab+Chl | ● Hbl+Act+Ab+Ep+Chl | | | |
| ▣ Prh+Ep+Ab+Chl | ● Hbl+Act+Ab+Olig+Ep+Chl | | Black = Probe Determined | |
| ▣ Pmp+Ep+Ab+Chl | ● Act+Olig+Ab+Ep+Chl | | Brown = Microscope Determined | |
| ▣ Prh+Pmp+Ep+Ab+Chl | ● Hbl+Act+Plag(?) +Ep+Chl | | | |

Metamorphic facies

- ▣ Transitional GS-Am Facies (Hbl-Olig Zone)
- ▣ Transitional GS-Am Facies (Act-Hbl-Olig Zone)
- ▣ Transitional GS-Am Facies (Act-Hbl Zone)
- ▣ Greenschist (GS) Facies
- ▣ Transitional PP - GS Facies
- ▣ Prehnite-Pumpellyite (PP) Facies
- ▣ Unknown Grade
- ▣ Missi Group Sediments
- ▣ Post Missi Intrusives

Structural features

- Fault
- Thrust Fault
- Fold
- Sample
- ⊕ Antiform
- ⊖ Synform
- ⊕ Overturned Synform
- VMS Deposit

remaining samples containing only prehnite. Prehnite is typically more abundant than pumpellyite, and in several samples pervasively replaces all components of the original basalt (groundmass, amygdules, and plagioclase phenocrysts). Chlorite and epidote are abundant in the majority of samples. The original igneous mineralogy rarely makes up more than 5% of the rock and in some samples prehnite and pumpellyite appear to directly replace the igneous minerals.

Prehnite and pumpellyite are found in several different textures: (a) within amygdules, commonly associated with chlorite (Figure 4c); (b) as replacements of matrix mineralogy (Figure 4a,b); and (c) as replacements and pseudomorphs of plagioclase phenocrysts (Figure 4d). Their development is highly irregular with some areas of basaltic matrix dominated by prehnite (Figure 4a) and others by pumpellyite (Figure 4b).

4.2 | Prehnite–pumpellyite—greenschist transition zone

The PP-GS transition is defined as the zone between the first development, in a prograde sense, of actinolite and last occurrence of prehnite and pumpellyite. The mineral assemblages within this zone are varied and individual samples are commonly domainal or patchy. The different mineral sub-assemblages comprise: (a) Prh+Pmp+Ab+Chl+Ep; (b) Act+Prh+Pmp+Ab+Chl+Ep; (c) Act+Pmp+Ab+Chl+Ep; (d) Act+Ab+Chl+Ep; and (e) Ab+Chl+Ep. The occurrence of actinolite with either or both of prehnite and pumpellyite is uncommon. Most samples contain either the diagnostic prehnite–pumpellyite zone assemblage (Prh+Pmp+Ab+Chl+Ep) or a typical greenschist facies assemblage (Act+Ab+Chl+Ep). Actinolite occurs in the matrix as fine euhedral needles intergrown with either or both of prehnite (Figure 4f) and pumpellyite (Figure 4e). Calcite is common, occurring in the matrix but more commonly as partial pseudomorphs after plagioclase phenocrysts and within amygdules.

4.3 | Greenschist facies

Rocks of the greenschist facies make up the majority of the field area, north of the prehnite/pumpellyite-out isograd and south of the hornblende-in isograd (Figures 2 and 3). The characteristic mineral assemblage of the greenschist facies is Act+Ab+Ep+Chl+Qtz+Ttn±Bt±Ms±Stp±Ksp±Ap. Clinopyroxene and plagioclase phenocrysts are pseudomorphed by actinolite and albite, respectively (Figure 5b), whereas amygdules most commonly consist of quartz, epidote, chlorite, and calcite. The first development of biotite, marking the biotite-in isograd, occurs in the lower part of the greenschist facies, close to the prehnite/pumpellyite-out isograd, although the fine grained nature of biotite in the lower grade samples makes determining the precise position difficult.

4.4 | Greenschist to amphibolite facies transition

In the field, this transition comprises a 4 km wide region containing the hornblende-in, oligoclase-in, and actinolite-out isograds that represent the low-grade margins of the hornblende–actinolite, hornblende–actinolite–oligoclase, and hornblende–oligoclase zones, respectively (Figures 2 and 3b).

4.4.1 | Hornblende–Actinolite Zone

Hornblende is only a minor component within the lower half of this zone, forming small (<10 μm) blebs developed sporadically within actinolite grains. Hornblende becomes more abundant in this zone in samples north of the Flin Flon townsite, and comprises more than 10% of the total amphibole content north of Hidden Lake, within 1 km of the oligoclase-in isograd.

4.4.2 | Hornblende–Actinolite–Oligoclase zone

This zone is marked by the appearance of oligoclase, and is characterized by the assemblage Hbl+Act+Olig+Ab+Ep+Chl+Qtz+Ilm+Ttn+Bt±Ms±Stp±Ksp±Ap. Rocks in this zone show more evidence of metamorphic recrystallization, with less common preservation of igneous microphenocryst textures in the matrix. Hornblende is identifiable in the field as 2–5 mm-long black needles just north of the oligoclase-in isograd, coarsening and increasing in abundance with increasing grade.

4.4.3 | Hornblende–Oligoclase Zone

The actinolite-out isograd is located within the northernmost part of the field area (Figures 2 and 3b), above which samples are dominated by hornblende, oligoclase, and epidote, with more minor albite and chlorite. Oligoclase makes up over 60% of the total plagioclase in these samples. Similar to the hornblende–actinolite–oligoclase zone, biotite is the dominant mica with only minor muscovite present. This zone represents the highest grade of metamorphism in the area, as the Hidden Formation basalts are in fault contact with the Missi Group sedimentary sequence.

5 | MINERAL CHEMISTRY AND MODAL PROPORTIONS

Mineral compositions and modal proportions were obtained using a JEOL JXA-8200 electron microprobe at the

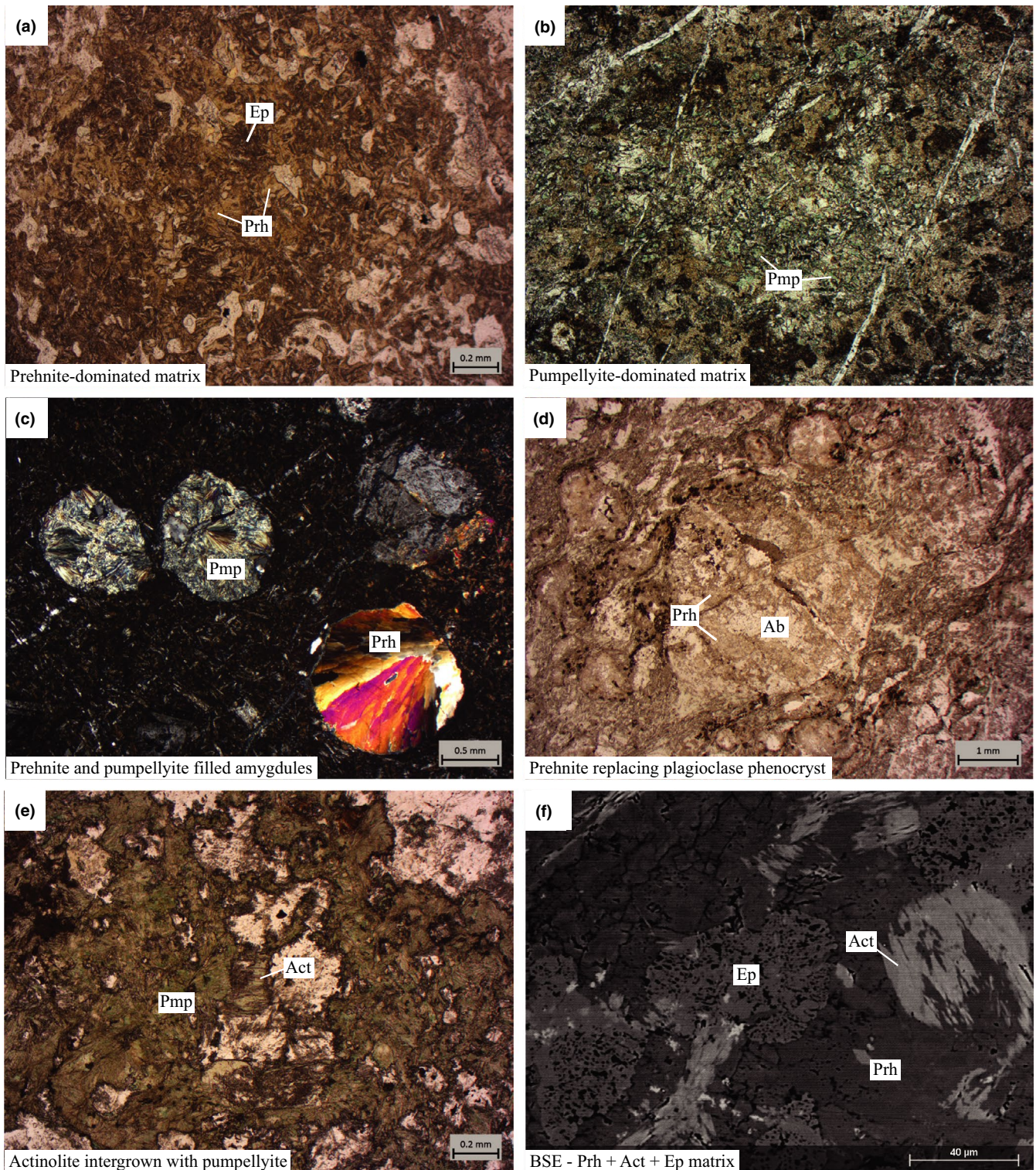


FIGURE 4 Photomicrographs of samples from the prehnite–pumpellyite facies and PP-GS transition zone. (a) Matrix dominated by light brown prehnite and dark brown epidote with clear quartz and minor green pumpellyite; (b) matrix containing pumpellyite (light green) and prehnite (light brown) with more minor epidote and quartz; (c) cross-polarized light image of prehnite and pumpellyite within amygdules; (d) prehnite and albite replacing plagioclase phenocryst; (e) actinolite intergrown with pumpellyite in prehnite–pumpellyite to greenschist transition zone; (f) small actinolite rhombs growing within prehnite- and epidote-dominated matrix

University of Calgary. Mineral proportions were determined by the following process: (a) back-scattered electron and EDS X-ray element compositional mapping; (b) construction

of composite BSE/X-ray maps by overlaying different combinations of EDS element distribution maps with BSE images, comprising as much of the thin section as possible

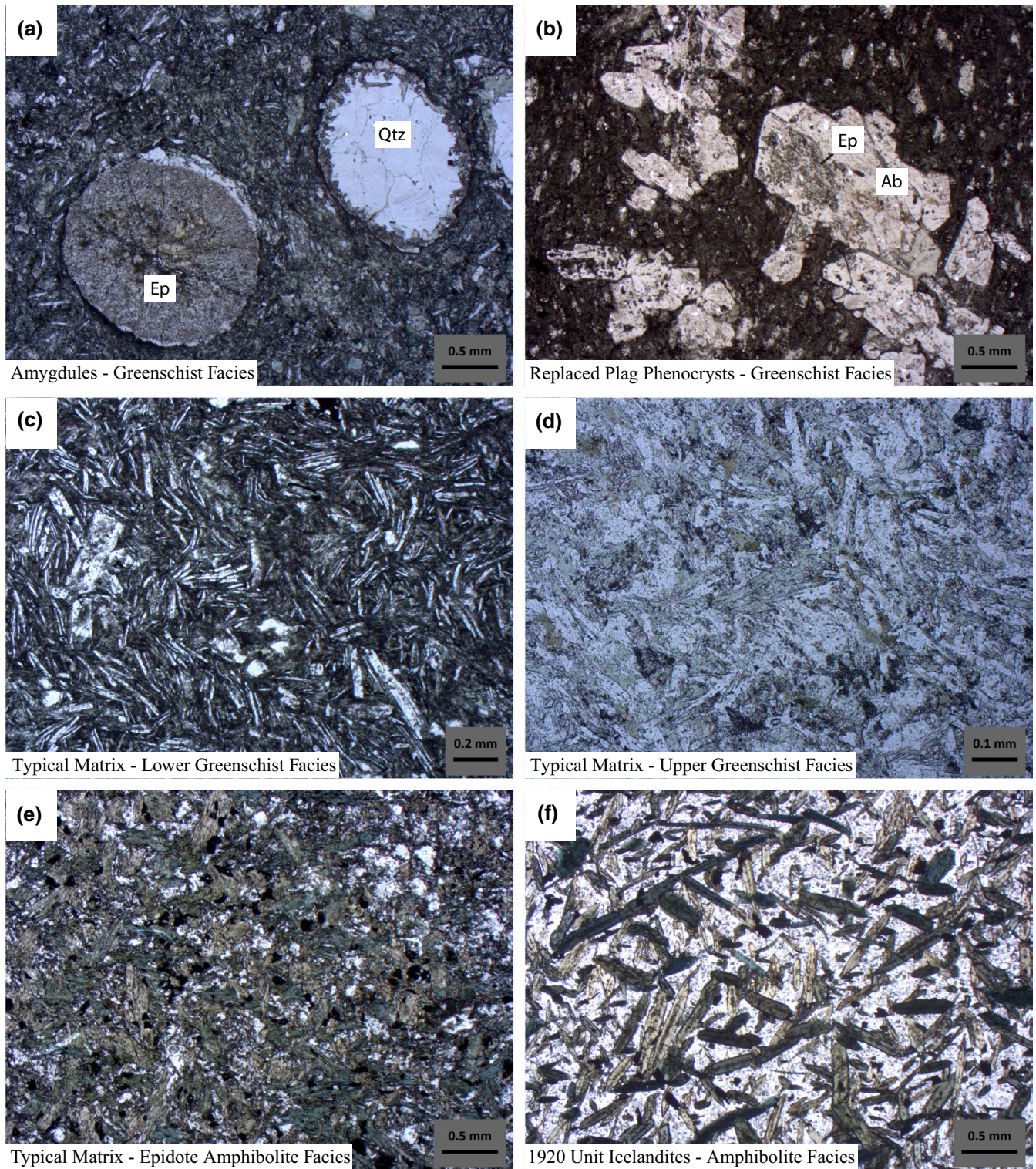


FIGURE 5 Photomicrographs of samples from the greenschist facies and greenschist–amphibolite transition zone. (a) Epidote and quartz in amygdules; (b) replacement of plagioclase phenocrysts within the greenschist facies—replacement assemblage of albite and epidote; (c) typical lower greenschist facies matrix preserving original igneous textures but with a mineralogy consisting of metamorphic albite, chlorite, epidote, and actinolite; (d) upper greenschist facies matrix with a coarser grained, more recrystallized matrix than that occurring in the lower greenschist facies; (e) transitional greenschist–amphibolite facies mineral assemblage dominated by blue-green hornblende intergrown with actinolite, with plagioclase and epidote in the finer grained interstitial areas between the amphibole grains; (f) amphibolite facies assemblage from the 1920 icelandite unit consisting of hornblende and plagioclase with minor epidote

while avoiding phenocrysts, pseudomorphs, and amygdules; and (c) determination of areas comprising different mineral phases by means of colour intensity threshold templates using the program JMicrovision. Mineral compositions were acquired from ~80 samples, while 50 samples were selected for full modal analysis using the methods described above. Variations in mineral compositional and modal data along a N–S transect through the Flin Flon sequence are shown in Figures 6 and 7. This N–S transect is taken to be a proxy for increasing grade as it occurs at a high angle to the E–W-oriented isograds. The complete modal data set is presented in Table S1, while mineral compositional data for amphibole, plagioclase, epidote, and chlorite are shown in Tables S2–S5, respectively.

5.1 | Amphibole

A detailed treatment of the variation in amphibole compositions and textures with grade across the GS-AM transition is described in Starr and Pattison (2019a), so only the main changes are reported in this paper. The amphibole stoichiometry, ferric iron content, cations per formula unit (cpfu) values, and site allocations were calculated following the methods of Schumacher (1997). For the classification of the amphiboles, the scheme of Hawthorne et al. (2012) was used.

Within the PP-GS transition, actinolite is present as fine acicular grains, generally only visible using scanning electron microscopy. Within the greenschist facies, actinolite becomes coarser grained, increases in abundance in the matrix, and is the dominant replacement mineral in pseudomorphs of clinopyroxene phenocrysts. Above the hornblende-in isograd, actinolite and hornblende occur together in a number of textural relationships, including separate individual homogeneous grains, patchy intergrowths, more geometrically regular intergrowths, and core-rim microstructures (usually hornblende rimming actinolite) (Starr & Pattison, 2019a).

Amphiboles from the PP-GS transition and greenschist facies show limited compositional variation and the majority of analyses classify as actinolite. Above the hornblende-in isograd, the amphibole compositions form two groups, separated by a distinct compositional gap (Figure 7a). The first group plots mostly as actinolite and is indistinguishable from actinolite that occurs at lower grades within the greenschist facies. The second group is composed predominantly of ferro-hornblende and ferro-tschermakite, with minor magnesio-hornblende, that for the purpose of this discussion will be loosely termed ‘hornblende’. The compositional difference between actinolite and hornblende is defined by higher A-site occupancy, ${}^{\text{C}}\text{Al}$, ${}^{\text{C}}\text{Ti}$, ${}^{\text{C}}\text{Fe}^{3+}$ and ${}^{\text{B}}\text{Na}$, and lower ${}^{\text{T}}\text{Si}$, $\text{Mg}^{2+}/\text{Mg}^{2+}+\text{Fe}^{2+}$ and ${}^{\text{B}}\text{Ca}$, in hornblende. The compositional gap appears to increase with grade, with the hornblende evolving from ferro-hornblende in the hornblende–actinolite–albite

zone to ferro-tschermakite in the hornblende–actinolite–oligoclase zone (Figure 7a).

5.2 | Plagioclase

Albite is generally present in high modal proportions within the prehnite–pumpellyite and greenschist facies and shows a modal decrease across the greenschist–amphibolite transition zone (Figure 6b). Within the hornblende–actinolite–oligoclase zone, two distinct plagioclase group minerals exist, one classifying as albite, with compositions ranging between $\text{An}_{1.1-5.8}$, and the other as oligoclase, with An contents ranging from $\text{An}_{17.5-26.0}$ (Figure 7b). Observations from BSE imaging show that coexisting albite and oligoclase occur both as separate grains and as finer intergrowths. The compositional transition at grain boundaries between coexisting feldspars appears to always be sharp and grain boundaries are generally more geometrically regular than those between coexisting amphiboles.

5.3 | Epidote

Epidote occurs throughout the Flin Flon sequence and shows a complex array of textures and compositions, with most samples containing different varieties of epidote group minerals with no systematic changes in composition with grade (Figure 7c). The most common texture, revealed by BSE imaging and observed in all of the metamorphic zones, is a core-rim microstructure comprising a light core surrounded by a darker rim reflecting different Fe contents. The light cores have X_{Fe} ($=\text{Fe}^{3+}/\text{Al}+\text{Fe}^{3+}$) contents of 24%–32%, whereas the darker rims have X_{Fe} contents of 17%–24% (Figure 7c).

5.4 | Chlorite

Chlorite persists to the highest grades in the Flin Flon sequence and is found in nearly all samples. Chlorite shows minor compositional variation in Mg, Fe, Al, and Si, with most chlorite slightly enriched in Fe relative to Mg with an average X_{Mg} ($=\text{Mg}/(\text{Mg}+\text{Fe}^{2+})$) of 0.42 within a range of 0.35–0.50 (Figure 7d). Chlorite compositions do not vary systematically with grade (Figure 7d).

5.5 | Titanite/Ilmenite

Titanite is present in most basaltic samples within the prehnite–pumpellyite, PP-GS transition, and greenschist facies. Above the oligoclase-in isograd, within the GS-AM transition ilmenite is stable and is the main Ti-bearing phase.

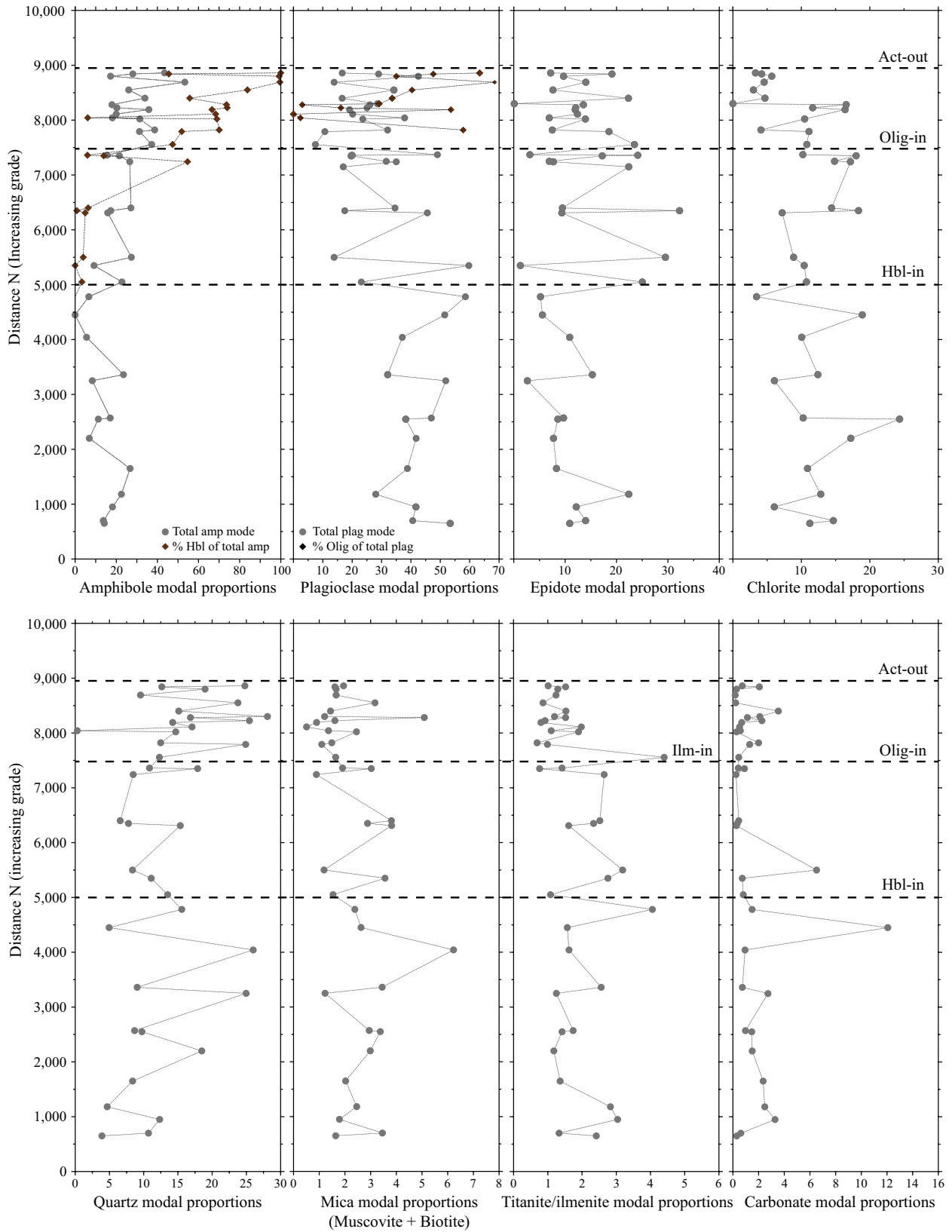


FIGURE 6 Plots of selected mineral modes versus distance north in metres, the latter a proxy for increasing metamorphic grade (see discussion in text), for samples across the greenschist facies and greenschist–amphibolite facies transition zone. The positions of the mineral isograds (hornblende-in, oligoclase-in, and actinolite-out) are shown by the dashed lines and correspond to the isograds shown in Figure 3b

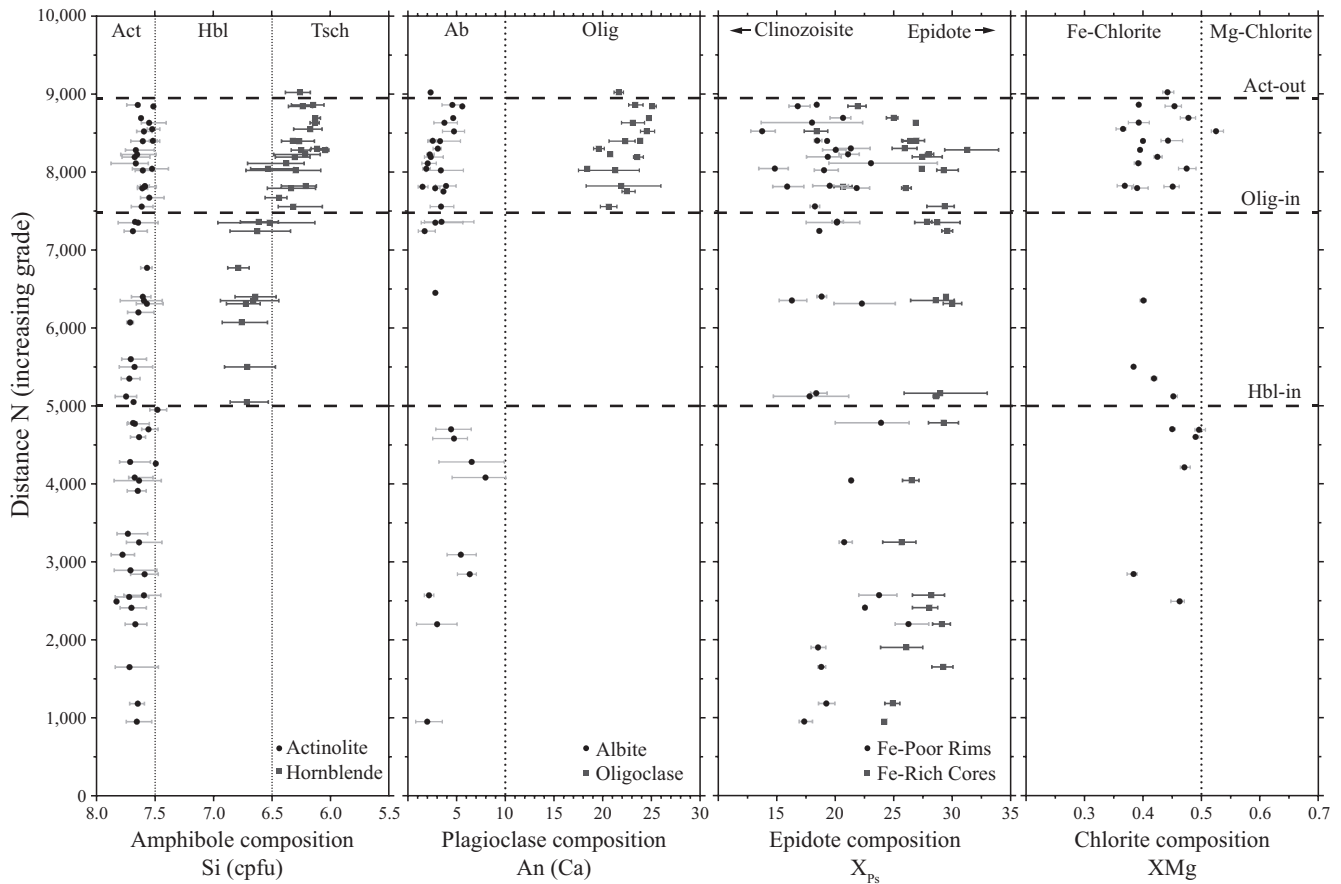


FIGURE 7 Plots of selected mineral compositional parameters versus distance north (m) for samples across the greenschist facies and greenschist–amphibolite facies transition zone. The points represent the average composition for that sample while the lines represent the full range of compositions observed. Compositional fields for amphibole after Leake et al. (1997)

However, it is commonly rimmed by titanite, which is interpreted to reflect retrograde growth of titanite at lower grades.

6 | BULK COMPOSITIONAL DATA

Major element bulk compositions were compiled for 129 samples and are listed in Table S6. The data were obtained from several sources: (a) 67 major and trace element bulk compositions from Ames et al. (2016); (b) eight major element XRF analyses, including ferrous iron titration; and (c) calculated bulk compositions from 54 samples, in which the mineral modal proportions were combined with mineral compositions obtained from the electron microprobe.

Figure 8 shows the bulk compositional data set plotted on ACF and CaO–Na₂O–MgO diagrams. For reference, the data set of Schilling et al. (1983), containing >200 bulk compositions from modern basalts dredged from the ocean floor, is also displayed to show the typical compositions for unaltered mid-ocean ridge basalts. The large amount of compositional variation is attributed predominantly to seafloor hydrothermal alteration processes that occurs prior to metamorphism. The data are divided into a number of groups: high-Mg, high-Ca,

and high-Na compositions (Figure 8b). The high-Mg and high-Ca compositions are typical of the pillow basalts of the Hidden and Louis Formations, with the high-Ca compositions representative of pillow cores and the high-Mg compositions characteristic of pillow rims. The complete bulk compositional database is shown in Table S6, and the average bulk compositions for the main groups (high-Mg, high-Ca, and high-Na) are presented in Table S7.

7 | THE PROGRADE EVOLUTION ACROSS THE PP-GS TRANSITION

7.1 | Observations from Flin Flon

Similar to observations from Digel and Ghent (1994) and Digel and Gordon (1995), the most distinctive feature of prehnite- and pumpellyite-bearing samples is the patchy development of different assemblages. Prehnite and pumpellyite vary from being absent or only a minor component of the rock to being developed pervasively as a replacement of the matrix, phenocryst, and amygdule components of the original basalt. In addition, the relationships between the proportions

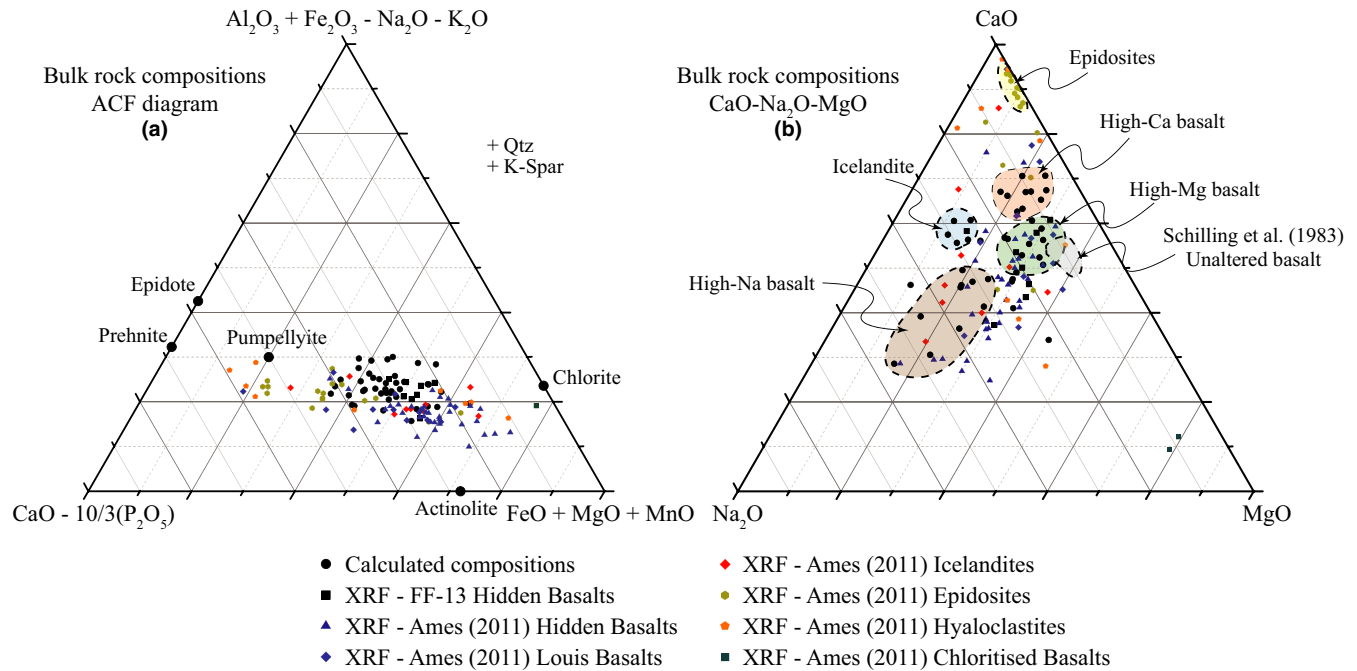
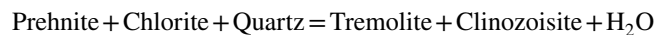
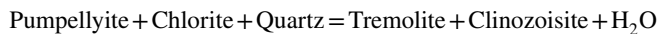


FIGURE 8 Bulk compositional data for metabasalts from the Flin Flon block including: (1) bulk compositions calculated using mineral modal and compositional data (black circles; see text for discussion); (2) XRF data collected by the author (“FF-13” data; black squares); and (3) bulk compositions from the open source database of Ames et al. (2011). (a) ACF diagram using molar proportions of oxide components; (b) CaO-Na₂O-MgO compositional plot; compositions described in terms of wt%

and distribution of actinolite, prehnite, epidote, and pumpellyite vary such that several different transitional assemblages occur within the same thin section.

The lower boundary of the PP-GS transition zone is marked by the appearance of actinolite that coexists with epidote and chlorite as part of typical greenschist facies assemblages or, more rarely, coexists with prehnite and/or pumpellyite. The following reactions, in the simplified Na₂O–CaO–MgO–Al₂O₃–SiO₂–H₂O (NCMASH) chemical system, have been suggested for the production of amphibole at the PP-GS transition zone (e.g. Day & Springer, 2005):



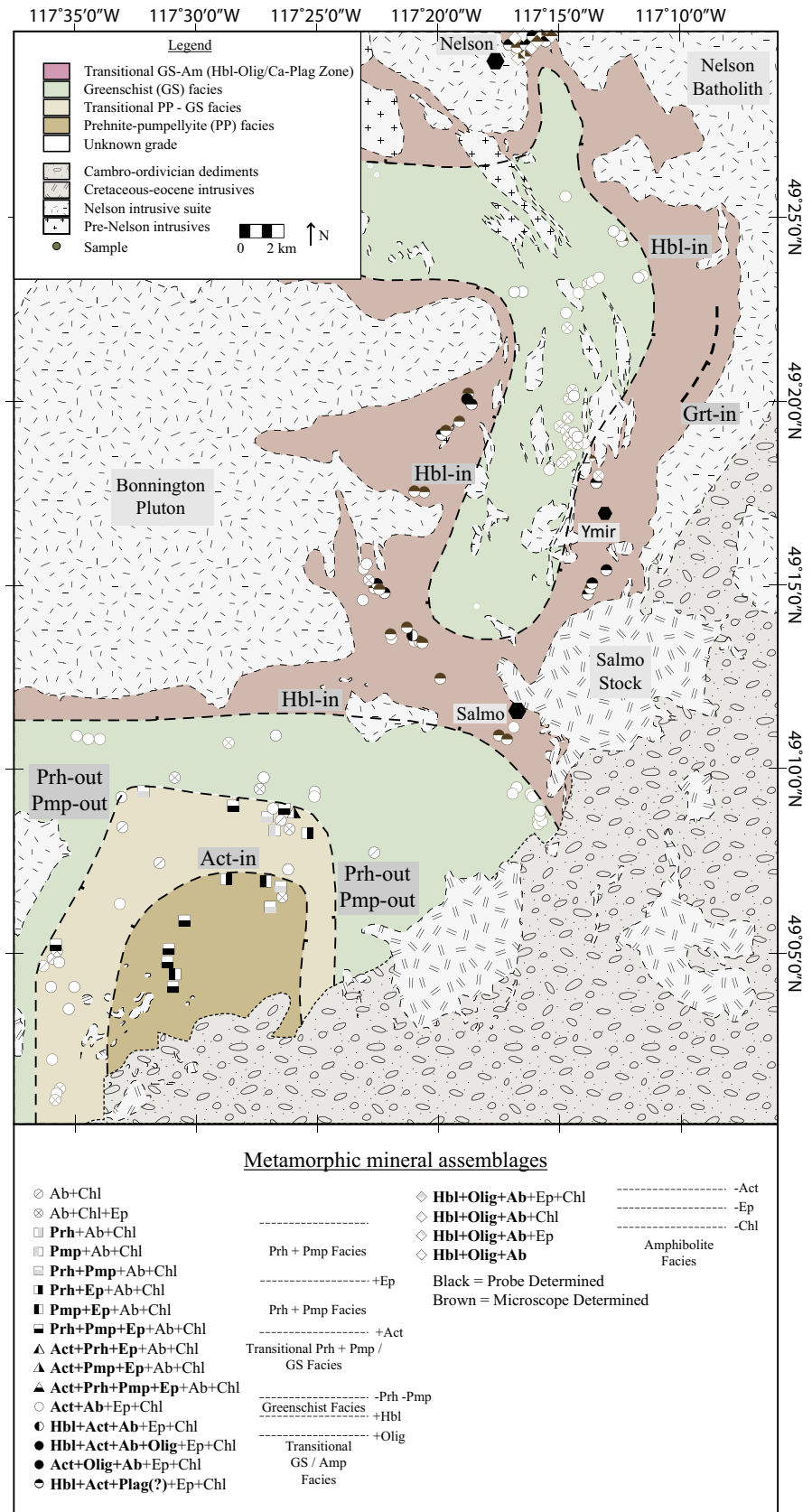
Intergrowths of actinolite with prehnite (Figure 4e) and pumpellyite (Figure 4f) suggest that both these reactions occur across the transition zone. The transition from prehnite–pumpellyite to greenschist facies assemblages occurs over a small interval within the field (<1,000 m; Figure 3a). Rather than containing the diagnostic transitional assemblage of actinolite coexisting with prehnite and/or pumpellyite, the majority of samples within the transition zone are typified by mineral assemblages characteristic of either the prehnite–pumpellyite facies (prehnite–pumpellyite–epidote–albite–chlorite) or the greenschist facies (actinolite–epidote–albite–chlorite)

(Figure 3a). These observations suggest that the reactions listed above occur in a narrow temperature interval and that the stability field of actinolite coexisting with prehnite and/or pumpellyite is small.

7.2 | Observations from other sequences

An examination of other examples of transitional PP-GS sequences from the literature (Bishop, 1972; Cho & Liou, 1987; Day & Springer, 2005; Digel & Ghent, 1994; Digel & Gordon, 1995; Powell, Carmichael, & Hodgson, 1993, 1995; Springer, Day, & Beiersdorfer, 1992; Starr & Pattison, 2019a) highlights some variation in the mineral assemblage evolution across the prehnite–pumpellyite to greenschist transition. Figure 9 shows a mineral assemblage map of a prehnite–pumpellyite to greenschist sequence from the Rossland area of British Columbia, described in Starr and Pattison (2019a). This sequence shows a similar pattern of mineral assemblages and textures to those observed at Flin Flon with a transition straight from prehnite–pumpellyite assemblages to a narrow transitional zone defined between the actinolite-in and prehnite- and pumpellyite-out isograds (Figure 9). As observed at Flin Flon, the majority of samples within this transition zone contain either a prehnite–pumpellyite facies assemblage (prehnite–pumpellyite–epidote–albite–chlorite), or greenschist facies assemblages (actinolite–epidote–albite–chlorite) (Figure 9), with prehnite and/or pumpellyite rarely coexisting with actinolite.

FIGURE 9 Regional metamorphic isograd map for the Rossland field area, superimposed on a simplified geology map. Mineral assemblages with a black rim or infill represent those documented using data from EDS and/or WDS analyses. Mineral assemblages indicated with a brown rim or infill are those determined by petrographic microscope only



The detailed study of Cho and Liou (1987) on the Karmutsen metabasites (Vancouver Island) also documented the persistence of both coexisting prehnite and pumpellyite through the

PP-GS transition zone up to the base of the greenschist facies, and only one of prehnite or pumpellyite was stable with actinolite within a single sample or thin section.

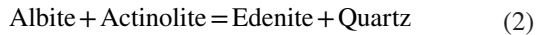
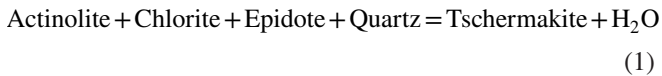
By contrast, isograd mapping of other sequences (e.g. Abitibi Greenstone Belt, Quebec; Smartville Complex, California) have recognized a more gradational transition from prehnite–pumpellyite to greenschist facies assemblages and the existence of a number of mineral assemblage subfacies. These studies documented the loss of pumpellyite before prehnite on a mappable scale and identified distinct prehnite–epidote and/or prehnite–actinolite mineral assemblage subzones (Powell, Carmichael, & Hodgson, 1993, 1995; Springer et al., 1992).

8 | THE PROGRADE EVOLUTION ACROSS THE GS-AM TRANSITION

8.1 | Observations from Flin Flon

8.1.1 | Hornblende–Actinolite Zone

The hornblende–actinolite zone is ~3.5 km wide and is characterized by hornblende coexisting with actinolite and albite (plus chlorite and epidote). The hornblende-producing reaction may be described by two simplified reactions in the NCFMASH chemical system that involve the breakdown of the typical greenschist facies mineralogy to form hornblende (described in terms of the tschermakite and edenite end-members) (e.g. Cooper, 1972; Graham, 1974):

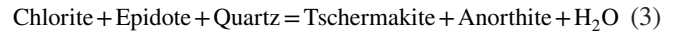


Where present, hornblende is generally in low modal abundance, comprising less than 20% of the total amphibole in the majority of samples (Figure 6a). There is no change in the modal proportions of other important minerals (e.g. epidote and chlorite) within this zone (Figure 6b–h). This suggests that although this zone is important in representing the first appearance of hornblende, and thus entry into the lower amphibolite facies, reaction progress is relatively modest and only accounts for a small proportion of the mineralogical transformation from a greenschist facies to amphibolite facies assemblage. The presence of coexisting actinolite and hornblende in this zone is interpreted to reflect stable coexistence across an actinolite–hornblende miscibility gap (e.g. Bégin & Carmichael, 1992; Brady, 1974; Schumacher, 2007; Starr & Pattison, 2019a).

8.1.2 | Hornblende–Actinolite–Oligoclase Zone

In addition to hornblende-producing reactions 1 and 2, further reactions involving the production of oligoclase are required

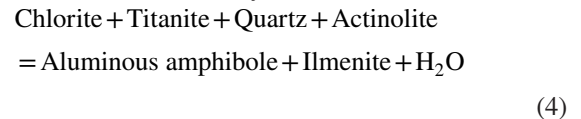
to explain the mineralogical changes within the hornblende–actinolite–oligoclase zone. The most commonly invoked oligoclase-producing reaction, described in the simplified NCFMASH system (e.g. Cooper, 1972; Graham, 1974), is:



This zone is characterized by a number of modal and compositional changes relative to the lower grade hornblende–actinolite zone (Figures 6 and 7). There is an average decrease of ~13 modal% in albite abundance accompanied by a smaller decrease in total plagioclase abundance, suggesting that the volume of oligoclase produced by the reactions within this zone is less than the volume of albite consumed. A large increase in the average hornblende abundance (+20 modal% average increase) is observed, with a corresponding decrease in the amount of actinolite. The total amphibole modal abundance increases (+15 modal% from the lower grade zones), while chlorite decreases by 7–11 modal% across the zone and epidote shows no consistent change in modal proportions. Actinolite is interpreted to be a metastable relict within this zone, based on textural observations such as actinolite cores surrounded by hornblende rims and the compositional evolution of both actinolite and hornblende (Starr & Pattison, 2019a).

The marked modal and compositional changes that occur through the hornblende–actinolite–oligoclase zone account for most of the mineralogical transition from greenschist facies to amphibolite facies assemblages. The narrow width of this zone in the field suggests that the main greenschist–amphibolite transition occurs over a relatively narrow temperature interval.

In addition to the changes noted above, the hornblende–actinolite–oligoclase zone is also characterized by the prograde replacement of titanite by ilmenite. The prograde appearance of ilmenite may be explained by the simplified schematic reaction (Liou, Kuniyoshi, & Ito, 1974):



The complete replacement of titanite by ilmenite occurs abruptly across the oligoclase-in isograd, suggesting marked reaction progress and the effective absence of a coexisting ilmenite–titanite field.

8.2 | Observations from other sequences

Previous studies of greenschist–amphibolite facies transition zone sequences have shown that, similar to that documented in Flin Flon, the transition is characterized by the appearance of hornblende and oligoclase, which

commonly coexists with actinolite and albite, and the loss or significant decrease in the amounts of epidote and chlorite. However, comparison of these different studies suggests that the order of isograds, particularly the order of the first appearances of hornblende and oligoclase, varies between different sequences. Examples of sequences in which oligoclase develops down-grade of hornblende include Northern Kiso District, Central Japan (Katada, 1965), and Karmutsen, British Columbia (e.g. Kuniyoshi & Liou, 1976; Terabayashi, 1993); whereas, examples of sequences in which hornblende develops down-grade of oligoclase include Haast River, New Zealand (Cooper & Lovering, 1970), SW Scottish Dalradian, Scotland (Graham, 1974), and N Quebec, Canada (Bégin, 1992; Bégin & Carmichael, 1992) and Flin Flon (this study). In other sequences, the incoming of hornblende and oligoclase has been interpreted as being coincident within the resolution of the sampling, including Yap Islands, western Pacific (Maruyama, Suzuki, & Liou, 1983), Kasuga, Japan (Maruyama et al., 1983), Sulitjelma, Norway (Boyle, 1986), and Rosslund, British Columbia (Starr & Pattison, 2019a).

9 | PHASE EQUILIBRIA MODELLING

Phase equilibria modelling of metabasic metamorphic rocks has traditionally proven to be difficult, due to the thermodynamic complexity of the common minerals in these rocks (e.g. amphibole, pyroxene, chlorite, and plagioclase). However, progress on the thermodynamic characterization of these minerals (e.g. Dale, Powell, White, Elmer, & Holland, 2005; Diener & Powell, 2012; Diener, Powell, White, & Holland, 2007; Green, Holland, & Powell, 2007) has allowed the modelling of metabasites within geologically realistic systems. In the following modelling and discussion sections, the GS-AM facies samples are discussed first as they are better characterized and are used to establish modelling inputs.

9.1 | Thermodynamic data sets and $a-x$ models

Phase diagrams for different bulk compositions were calculated using the Gibbs free energy minimization modelling software, Theriak-Domino (de Capitani & Brown, 1987; De Capitani & Petrakakis, 2010). In order to fully test the ability of the modelling data sets to reproduce natural observations, two different internally consistent thermodynamic data sets were used: data set 5 (referred to as 'DS5') of Holland and Powell (1998; updated to version DS5.5)

and data set 6 ('DS6') of Holland and Powell (2011; updated to version ds6.2). Each of these data sets were combined with compatible $a-x$ models. The $a-x$ models used with DS5 are as follows: clino-amphibole (Diener & Powell, 2012; Diener et al., 2007), clinopyroxene (Diener & Powell, 2012; Green et al., 2007), garnet (White, Powell, & Holland, 2007), chloritoid (White, Powell, Holland, & Worley, 2000), chlorite (Holland, Baker, & Powell, 1998), white mica (Coggon & Holland, 2002), biotite (White et al., 2007), epidote (Holland & Powell, 1998), spinel (White, Powell, & Clarke, 2002), ilmenite-hematite (White, Pomroy, & Powell, 2005; White et al., 2000), and feldspar (Holland & Powell, 2003). With DS6, the following $a-x$ models were used: clino-amphibole (Green et al., 2016), clinopyroxene (Green et al., 2016), garnet (White, Powell, Holland, Johnson, & Green, 2014), chlorite (White et al., 2014), white mica (White et al., 2014), biotite (White et al., 2014), epidote (Holland & Powell, 2011), spinel (White et al., 2002), ilmenite-hematite (White et al., 2005, 2000), and feldspar (Holland & Powell, 2003).

9.2 | Bulk compositions used for thermodynamic modelling

The average high-Mg composition is chosen for the thermodynamic modelling in the following sections because it is the most common composition sampled from the Hidden and Louis Formations and is most similar to the unaltered basaltic compositions of Schilling et al. (1983). Recent attempts at modelling metabasites at a range of different $P-T$ conditions have highlighted the strong control that ferric iron has on phase relations (e.g. Diener & Powell, 2010, 2012; Rebay, Powell, & Diener, 2010). For modelling purposes and in the following discussion, the ferric iron is expressed in terms of the wt% oxide ratio ($X_{\text{Fe}^{3+}} = \text{Fe}_2\text{O}_3/\text{Fe}_2\text{O}_3 + \text{FeO}$) in order to facilitate comparison with natural data sets, which are most often described in wt% oxides. The FeO and Fe_2O_3 contents of eight selected samples spanning the greenschist and lower amphibolite facies were determined using chemical titration combined with XRF at ACME labs in Vancouver. The $X_{\text{Fe}^{3+}}$ values vary between 20% and 36% with an average of 26.2%. The results derived from titration are interpreted as representing maximum estimates of $X_{\text{Fe}^{3+}}$ during metamorphism, due to potential oxidation during weathering, post-metamorphic alteration, and sample preparation (e.g. Diener & Powell, 2010; Lo Pò & Braga, 2014). The average $X_{\text{Fe}^{3+}}$, calculated through combining mineral modal data with their stoichiometric compositions, is 18.9% within a range of 5%–33% (equivalent to ~2 to 17 mol.% $\text{Fe}_2\text{O}_3/\text{Fe}_2\text{O}_3 + \text{FeO}$), although the majority of samples (~80%) have values between 10% and 25%. Calculated values of $X_{\text{Fe}^{3+}}$ are lower

(−7% average) than those derived from titration, consistent with minor amounts of post-metamorphic oxidation.

While the approaches for estimating ferric iron contents described above have helped constrain the approximate values of $X_{\text{Fe}^{3+}}$ for the Flin Flon sequence, there is a likely a range of different possible ferric iron contents for different bulk compositions. Thus, the approach of Diener and Powell (2010) is taken whereby the effects of ferric iron content on the phase equilibria are investigated through the calculation of sets of P – T diagrams with different $X_{\text{Fe}^{3+}}$ (Figures 10 and 12), augmented with T – $X_{\text{Fe}^{3+}}$ diagrams (Figure 11). A range of $X_{\text{Fe}^{3+}}$ contents of 0%–30%, representing the majority of the Flin Flon samples, was chosen for the construction of T – $X_{\text{Fe}^{3+}}$ diagrams while $X_{\text{Fe}^{3+}}$ values of 10% and 20% as well as the average calculated value, 16.9%, were used for constructing individual P – T diagrams.

9.3 | Modelling of the greenschist–amphibolite facies transition zone

The P – T and T – $X_{\text{Fe}^{3+}}$ phase diagrams, calculated for a range of P – T conditions spanning the GS-AM transition zone (400–550°C; 1–8 kbar), are shown in Figures 10 and 11 respectively. A constant pressure of 4 kbar was chosen for the calculation of the T – $X_{\text{Fe}^{3+}}$ phase diagrams as it falls within the range of most likely pressures discussed in more detail below. For ease of comparison, the fields are coloured corresponding to important groups of mineral assemblages across the GS-AM transition zone: blue (coexisting albite and oligoclase/andesine); brown (coexisting actinolite and hornblende); yellow (epidote–amphibolite—ep+hbl); green (chlorite-bearing, epidote-absent transitional assemblages—hbl+chl); and pink (coexisting actinolite and oligoclase with no hornblende—act+olig).

The P – T phase diagrams calculated for different values of $X_{\text{Fe}^{3+}}$ using DS5 and the corresponding a – x models (Figure 10a,c,e) show a number of similar features. A large field containing the greenschist facies assemblage Act–Chl–Ep–Ab occupies most of the phase diagram below 450°C (except at low pressures). Two relatively thin fields containing coexisting actinolite and hornblende, and coexisting albite and oligoclase, occur immediately up-grade of the greenschist facies field, which together correspond to the observed changes across the greenschist–amphibolite facies transition

zone. The compositional fields that comprise the epidote–amphibolite facies, defined by the coexistence of epidote and hornblende, narrow in size with decreasing pressure (Figure 10c,e).

The P – T phase diagrams calculated using DS6 (Figure 10b,d,f) show a number of differences compared with those calculated using the DS5 data set including: (a) a displacement of the plagioclase-in (andesine) reaction to higher temperatures; (b) a large increase in the size of the coexisting albite–oligoclase/andesine field (shown in blue); (c) a smaller coexisting actinolite–hornblende field (shown in brown); (d) displacement of the chlorite-out reaction to lower temperatures; and (e) a displacement of the ilmenite-in and titanite-out reactions to higher temperature. The result is a considerably different predicted sequence of mineral appearances and disappearances, with oligoclase appearing only at higher grades after the disappearance of one or both of chlorite and epidote at moderate pressures. In addition, the intersection of the hornblende-in and oligoclase/andesine-in lines occurs at very low pressures (~1 kbar) resulting in the absence, or much reduced size, of a field in which oligoclase/andesine coexists with actinolite rather than hornblende.

A number of consistent changes are observed with increasing $X_{\text{Fe}^{3+}}$ for phase diagrams calculated using either DS5 or DS6 (Figures 10 and 11): (a) the Act+Hbl field is displaced to lower temperatures; (b) the coexisting Ab+Pl field moves to slightly higher temperatures; and (c) there is an increase in the size of the epidote–amphibolite facies. These effects cause the intersection of the hornblende-in and oligoclase/andesine-in reactions to be displaced from ~4.7 kbar at 10% $X_{\text{Fe}^{3+}}$ (Figure 10a) to ~2.4 kbar at 20% $X_{\text{Fe}^{3+}}$ (Figure 10e) for the phase diagrams calculated using DS5, and from ~1.5 kbar at 10% $X_{\text{Fe}^{3+}}$ (Figure 10b) to <1 kbar at 20% $X_{\text{Fe}^{3+}}$ (Figure 10f) for the DS6 phase diagrams.

To provide an indication as to the metamorphic pressures during greenschist–amphibolite metamorphism at Flin Flon, the grey band on each phase diagram provides the closest match to the observed sequence of isograds: (a) the hornblende-in isograd appearing down-grade of the oligoclase-in isograd; and (b) actinolite-out up-grade of oligoclase-in. The estimated pressure varies considerably based on the ferric iron content for the DS5 phase diagrams (Figure 10a,c,e) but is restricted to the range of 3.3–4.3 kbar for the phase diagram calculated using the preferred average estimate for the ferric iron content (Figure 10c). For

FIGURE 10 P – T pseudosections calculated using DS5 (left) and DS6 (right) for different $X_{\text{Fe}^{3+}}$ contents: 10% (a, b), 16.9% (c, d), and 20% (e, f). All diagrams were calculated using the average high-Mg basaltic bulk composition. The thermodynamic data and a – x models used to calculate the diagrams are discussed in the text. The fields are coloured according to important mineral associations (discussed in the text): blue = coexisting albite and oligoclase; brown = coexisting actinolite and hornblende; yellow = epidote–amphibolite facies (coexisting epidote and hornblende); green = chlorite-bearing transitional assemblages (coexisting chlorite and hornblende); and pink = actinolite–oligoclase fields. The grey-coloured bands indicate the estimated pressure range for the Flin Flon sequence based on the observed sequence of isograds (see text for discussion)

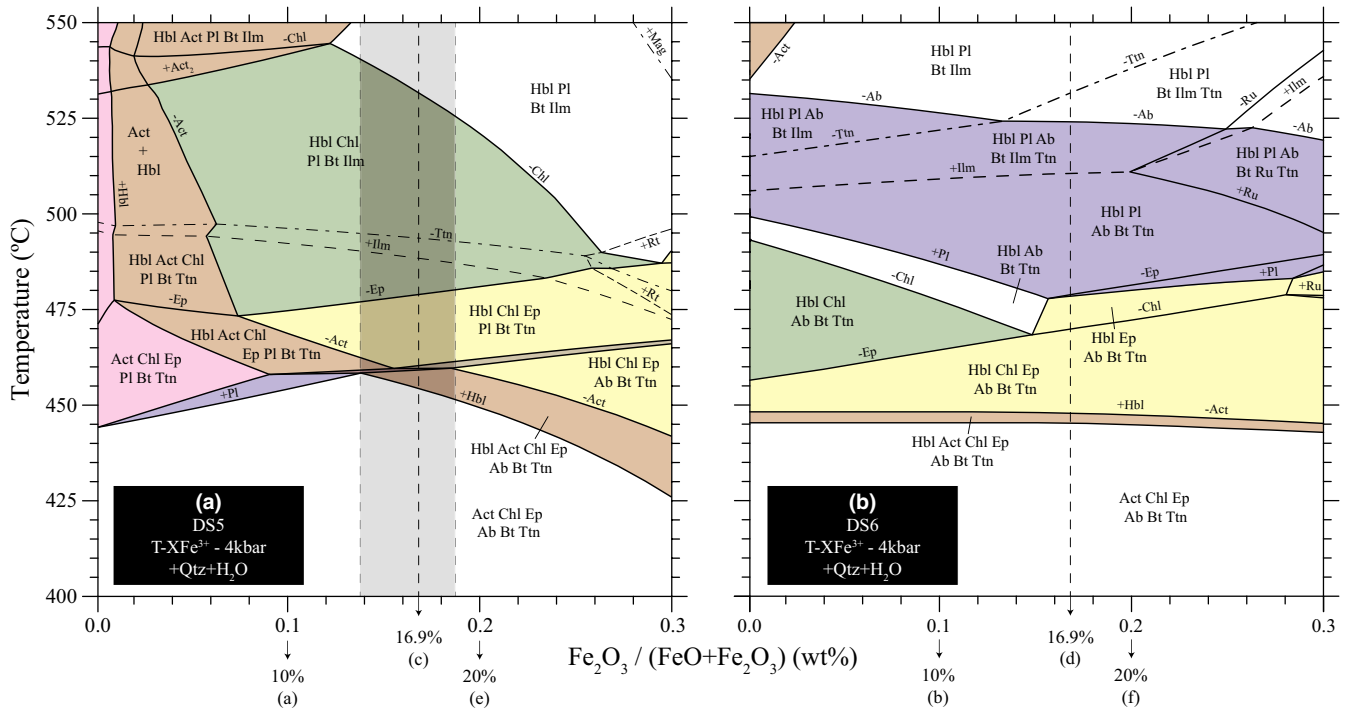


FIGURE 11 T - $X_{\text{Fe}^{3+}}$ diagrams calculated for greenschist to lower amphibolite facies conditions using DS5 (a) and DS6 (b), at a pressure of 4 kbar. The grey box in (a) represents the range of possible pressures that produce the correct sequence of isograds observed in Flin Flon (no such correct sequence occurs when modelling using DS6 in (b)). The labelled $X_{\text{Fe}^{3+}}$ values and letters below the x-axis refer to the P - T diagrams shown in Figure 10

the phase diagrams calculated using DS6, the range of estimated pressures for Flin Flon is much lower (1.5–1.8 kbar at 10% $X_{\text{Fe}^{3+}}$, 1–1.2 kbar at 16.9% $X_{\text{Fe}^{3+}}$, and <1 kbar at 20% $X_{\text{Fe}^{3+}}$).

9.4 | Modelling of the prehnite–pumpellyite–greenschist facies transition

Previous studies of prehnite–pumpellyite facies rocks have focussed on equilibria within the CMASH and NCMASH systems (Frey, Capitani, & Liou, 1991; Liou, Maruyama, & Cho, 1985; Powell, Carmichael, & Hodgson, 1993) due to the lack of thermodynamic data and a - x models for key phases such as prehnite and pumpellyite. However, as a number of minerals incorporate Fe^{2+} (pumpellyite, amphibole) and Fe^{3+} (prehnite, pumpellyite, amphibole, epidote), modelling in NCKFMASHTO is preferable in order to more realistically describe the natural phase equilibria.

Data set 5 does not include ferrous or ferric iron end-members for prehnite and pumpellyite, limiting the chemical system which can be modelled to NCMASH. However, the addition to DS6 of ferrous and ferric iron end-members for pumpellyite and a ferric iron end-member for prehnite, accompanied by new a - x models for these two minerals (Holland & Powell, 2011), allows the system to be expanded to NCKFMASHTO. A number of phase

diagrams were calculated at prehnite–pumpellyite to greenschist facies conditions (180–360°C; 1–5 kbar) using the same average high-Mg basaltic bulk composition described above.

The fields pertaining to the prehnite–pumpellyite and PP-GS transition facies are coloured according to the mineral sub-assemblages involving prehnite, pumpellyite, epidote, and actinolite: (a) prehnite–pumpellyite (red); (b) prehnite–epidote (yellow); (c) pumpellyite–actinolite (green); (d) prehnite–actinolite (dark blue); and (e) prehnite–epidote–actinolite (light blue). These different sub-assemblages are largely consistent with the common facies divisions (prehnite–pumpellyite, prehnite–actinolite, prehnite–epidote, and pumpellyite–actinolite) proposed for sub-greenschist metabasites (Frey et al., 1991; Liou et al., 1985; Powell et al., 1993).

Figure 12a shows a phase diagram calculated using DS5 in the NCMASH system. The prehnite–pumpellyite facies assemblage forms a relatively narrow field bounded by the prehnite-out/actinolite-in and the pumpellyite-out/clinozoisite-in univariant reactions. The pumpellyite–actinolite stability field occupies much of the phase diagram, whereas actinolite is not stable with prehnite in any part of the phase diagram. An invariant point, equivalent to the CHEPPAQ point (coexisting chlorite– H_2O –epidote–prehnite–pumpellyite–actinolite–quartz) of Powell et al. (1993), occurs at ~3.2 kbar, 295°C, separating higher pressure assemblages

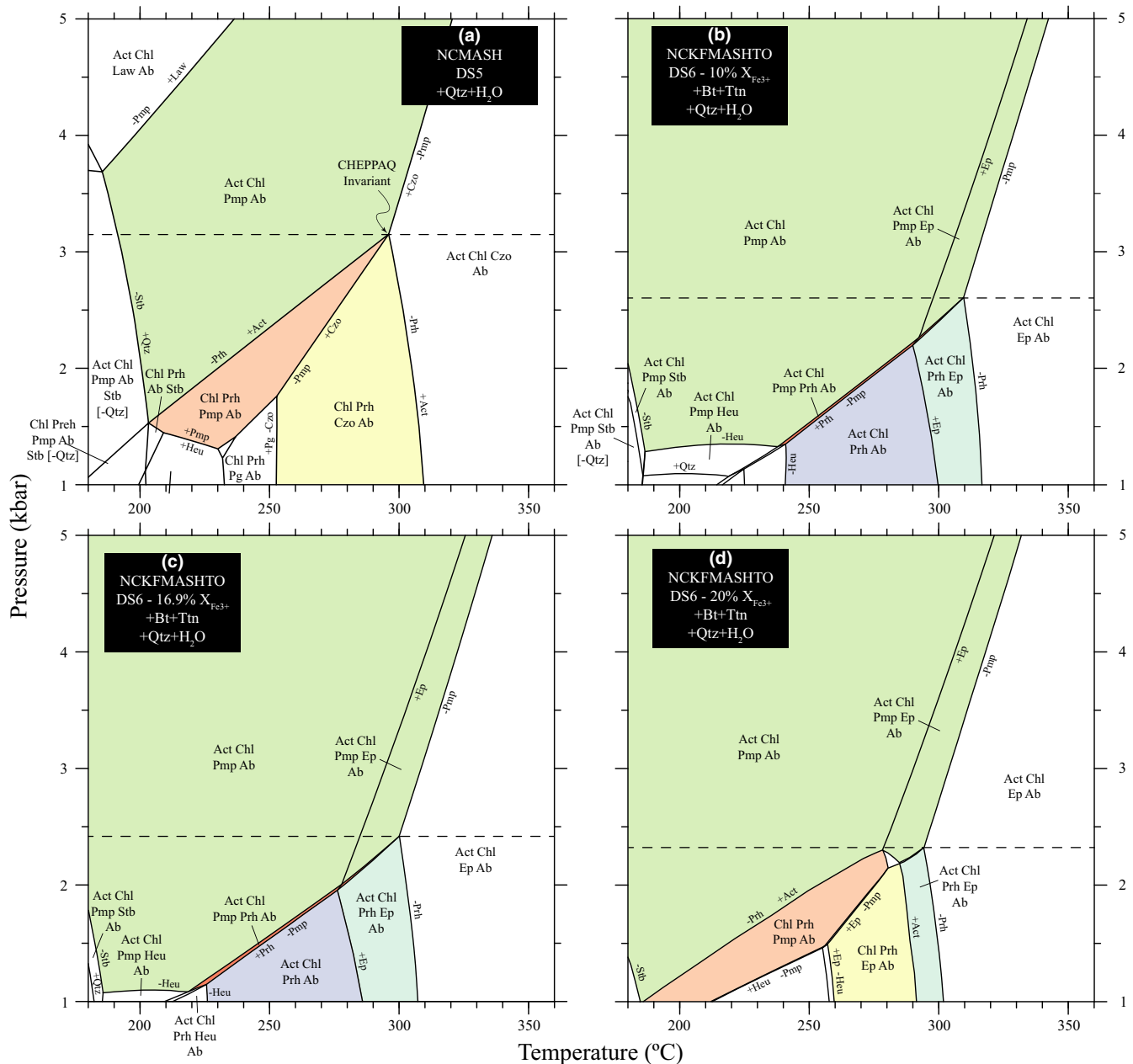


FIGURE 12 Thermodynamically calculated equilibrium P - T phase diagrams calculated for the average high-Mg basaltic bulk composition for prehnite–pumpellyite and greenschist facies conditions. The PP-GS transitional fields are coloured according to important mineral associations: prehnite–pumpellyite (red); prehnite–epidote (yellow); pumpellyite–actinolite (green); prehnite–actinolite (dark blue); and prehnite–epidote–actinolite (light blue). The dashed line represents the maximum pressure at which prehnite would be stable. (a) Phase diagram calculated in NCMASH using DS5; (b)–(d) phase diagrams calculated in NCKFMASHTO using DS6 with $X_{\text{Fe}^{3+}}$ values of 10% (b), 16.9% (c), and 20% (d)

which would have a prograde evolution from pumpellyite–actinolite to greenschist facies from lower pressure sequences passing through the pumpellyite–actinolite, prehnite–pumpellyite, and prehnite–epidote facies with increasing grade.

The inclusion of ferric and ferrous iron and the expansion of the chemical system to NCKFMASHTO using DS6 results in a number of changes to the topology of the phase diagrams (Figure 12b–d). When modelling with $X_{\text{Fe}^{3+}}$ values of 10% (Figure 12b) and 16.9% (Figure 12c), actinolite is

stable across the full range of P - T space and prehnite and pumpellyite only coexist (with actinolite) within a very narrow field. By contrast, the phase diagram calculated with an $X_{\text{Fe}^{3+}}$ of 20% (Figure 12d) results in phase equilibria that more closely resemble observations from Flin Flon and other similar sequences, including a large prehnite–pumpellyite facies field (red), and a transitional field containing coexisting prehnite and actinolite (light blue). The increase in ferric iron stabilizes epidote and pumpellyite relative to actinolite.

10 | COMPARISON BETWEEN MODELLING RESULTS AND OBSERVATIONS

10.1 | Greenschist to amphibolite facies transition

The detailed documentation of mineral assemblages, modal proportions, and compositions from Flin Flon, combined with a database of observations from other sequences, allows for the evaluation of modelling results generated using both DS5 and DS6. The modelling using DS5 is able to broadly reproduce the main observations from Flin Flon and other sequences. This includes reproducing the sequence of isograds from the Flin Flon sequence and the presence of different mineral assemblage sequences at different pressures, and is therefore useful for examining P - T conditions and petrogenetic processes in these rocks. However, a number of differences exist between the model results produced using DS5 and the natural observations: (a) differences in the compositions of key minerals such as amphibole and chlorite; (b) sensitivity to $X_{\text{Fe}^{3+}}$ content, which is not supported by natural observations; and (c) differences between the observed stability of ilmenite, which first appears coincident with the oligoclase-in isograd, and the predicted stability field, which occurs considerably up-grade of the hornblende-in and oligoclase-in reactions.

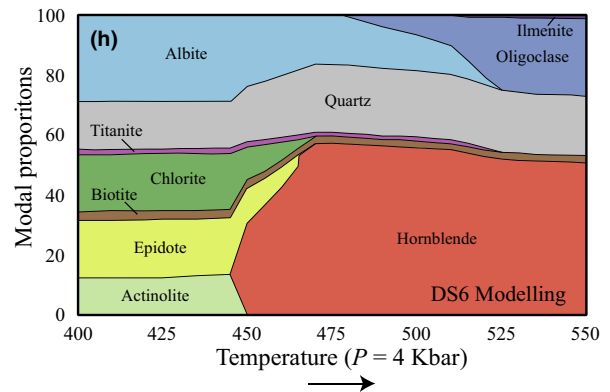
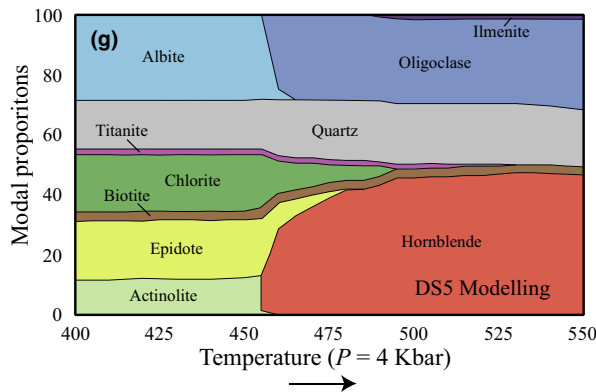
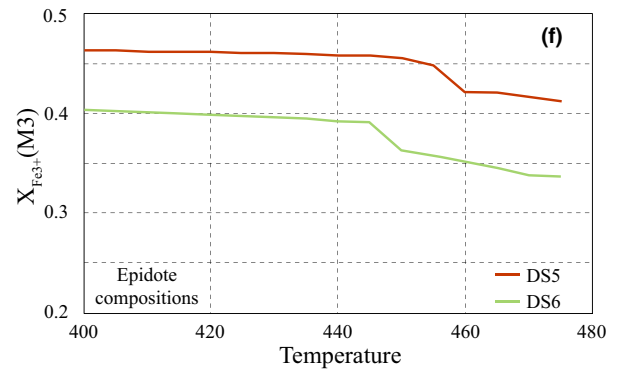
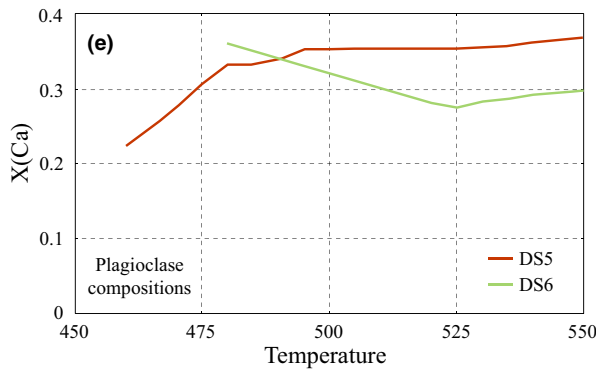
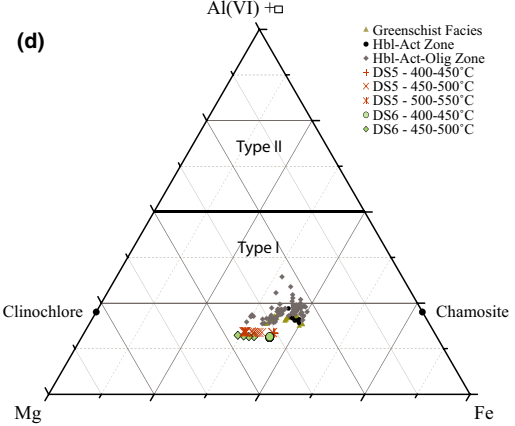
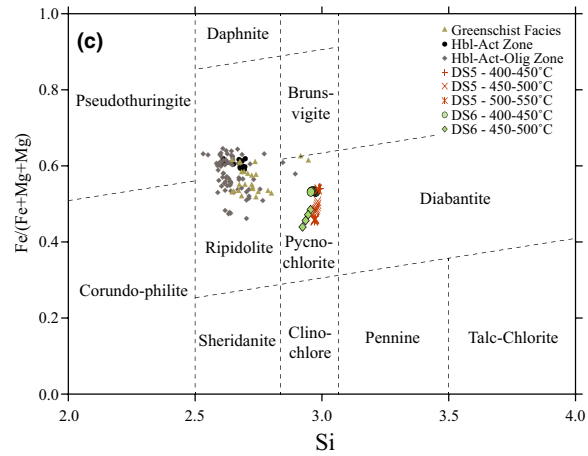
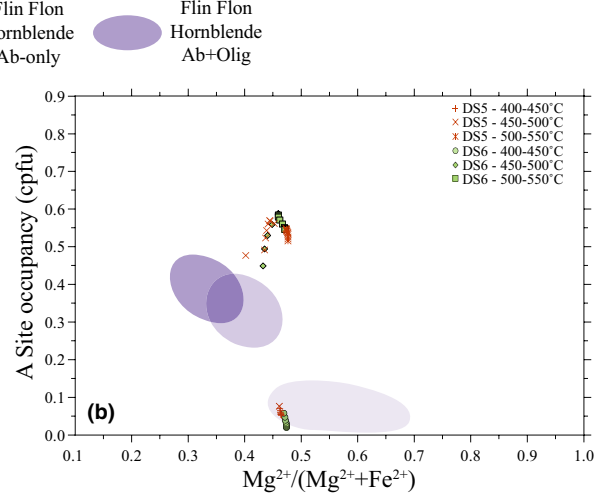
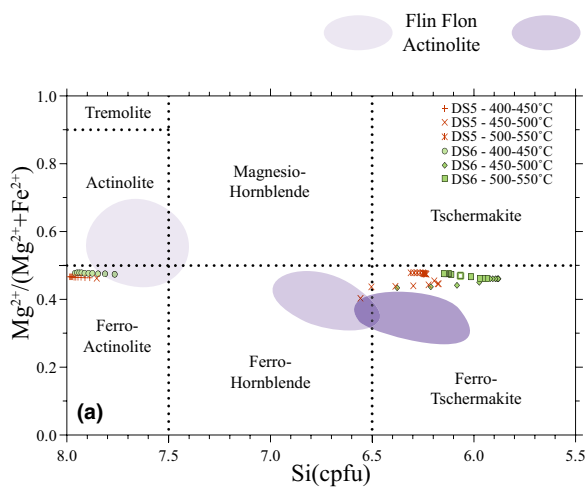
By contrast, the modelling results using DS6 show a number of important differences from those using DS5, a number of which are incompatible with observations from Flin Flon and other sequences. Perhaps the most important difference concerns the relative stability and compositions of amphibole and plagioclase group minerals. The appearance of oligoclase/andesine and the disappearance of albite are predicted to occur at much higher temperatures than the hornblende-in reaction at moderate pressures, and the field of coexisting albite and oligoclase/andesine occupies a much larger area of P - T space. A comparison of the changing modal abundances with increasing temperature (at 4 kbar) calculated using DS5 versus DS6 is shown in Figure 13g,h. This shows that for the DS5 modelling, the appearance of oligoclase and hornblende occurs concurrently with the breakdown of actinolite, epidote, albite, and chlorite over a narrow range of

temperature (Figure 13g). By contrast, modelling using DS6 predicts the formation of more calcic plagioclase (initially andesine; Figure 13e) at higher temperatures, after the major hornblende-forming reaction and dehydration interval, involving the breakdown of albite and a small amount of hornblende. Based on the observed modal abundance changes in Flin Flon, the DS5 modelling does a more realistic job of reproducing the observed patterns of mineral isograds and reactions in Flin Flon and other sequences from the literature.

In addition, the predicted compositions of important minerals, particularly hornblende, generated using DS6 are different than those observed at Flin Flon and predicted using DS5. Figure 13a-f show a comparison between measured and calculated compositions of amphibole, chlorite, plagioclase, and epidote using data sets 5 and 6, calculated along an isobaric P - T path from 400 to 550°C at 4 kbar (compositions calculated every 5°C). The predicted amphibole compositions generated using DS5 are closer to those observed in the Flin Flon sequence, with the amphibole compositions for the DS6 modelling containing too little Si (and hence high $^{\text{T}}\text{Al}$) by ~ 0.2 – 0.9 cpfu (Figure 13a). The predicted A-site occupancies are higher than those observed at Flin Flon, for both the DS5 and DS6 modelling by ~ 0.05 – 0.25 cpfu (Figure 13b). These differences are similar to those documented by Forshaw, Waters, Pattison, Palin, and Gopon (2019), who compared observed and thermodynamically predicted compositions of amphibole in mafic granulites using DS6.

The discrepancies between the modelling results produced using DS5 and DS6 are likely a function of changes to both the plagioclase and amphibole a - x models. Modifications to the plagioclase a - x models for DS6 appear to result in the stability fields for the more calcic plagioclase phase being shifted to higher temperatures and an increase in the anorthite content of the plagioclase such that the stable plagioclase coexisting initially with albite is andesine (e.g. An_{36} ; Figure 13e) rather than oligoclase. The amphibole a - x models likely also play a role in controlling the relative stability fields of amphibole and plagioclase, with the unusually high predicted Al contents (Figure 13a) and higher modal proportions (Figure 13h) of the hornblende potentially suppressing the appearance of more calcic plagioclase (andesine) such that it only appears at higher temperatures. Based on this analysis of the DS6 modelling, it is suggested that some modifications to the

FIGURE 13 Comparison of analysed mineral compositions from the Flin Flon sequence with predicted compositions using DS5 and DS6 for amphibole (a, b), chlorite (c, d), plagioclase (e) and epidote (f) and a comparison of the predicted modal abundances for DS5 (g) and DS6 (h). Mineral compositions were calculated along an isobaric P - T path from 400 to 550°C at 4 kbar (compositions calculated every 5°C). (a, b) Predicted versus analysed amphibole compositions. The shaded areas show the amphibole compositions from the greenschist facies (lightest shade), hornblende-actinolite zone (medium shade), and the hornblende-actinolite-oligoclase zone (darkest shade). The symbols represent compositions calculated at different temperatures (see key). (c) Si versus Fe/(Fe+Mg) ratio plot for chlorite (plot and fields after Hey, 1954). (d) Octahedral cation plot for chlorite (plots and fields after Zane and Weiss, 1998). (e) Comparison of plagioclase compositions (X_{Ca} —anorthite content) versus temperature for DS5 and DS6. (f) Comparison of epidote composition ($X_{\text{Fe}^{3+}}$ (M3)) versus temperature for DS5 and DS6. (g, h) Predicted modal abundances with increasing temperature for DS5 (g) and DS6 (h)



plagioclase and amphibole $a-x$ models, the latter of which was calibrated using higher grade metabasic granulites, are likely required in order to accurately model mafic rocks at greenschist and amphibolite facies conditions.

In this study, exploratory modelling was conducted to test whether the new addition of Ti and K to the DS6 amphibole models has a significant effect on the phase diagram topology, calculating phase diagrams, and mineral compositions for an average high-Mg basaltic bulk composition, with Ti and/or K excluded from the amphibole models of Green et al. (2016) (Figure S1). The phase diagrams and predicted mineral compositions are very similar regardless of the presence or absence of Ti and/or K, suggesting that the source of the discrepancies lies elsewhere (Figure S1). It may be that changes to the thermodynamic end-member data or mixing properties that influence the degree of tschermakite substitution are the main cause of the discrepancies.

One of the noteworthy features of the thermodynamic modelling of this study is the large effect that ferric iron content has on the stability of amphibole and epidote minerals, and thus on the relative positioning of the hornblende-in and oligoclase-in reactions. Even small changes in the ferric iron contents, such as by varying $X_{\text{Fe}^{3+}}$ between 10% and 20%, affects the predicted order of reactions as well as the pressure of the hornblende–oligoclase intersection (Figures 10 and 11). Given the regularity in mineral assemblage sequences in Flin Flon, where samples display a range of ferric iron contents ($X_{\text{Fe}^{3+}} = 5\text{--}33\%$), and other similar sequences described in the literature, the thermodynamically predicted sensitivity of the phase equilibria to small variations in whole-rock ferric iron content seems inconsistent with the repeatable natural observations and likely reflects some oversensitivity of the $a-x$ models to the $X_{\text{Fe}^{3+}}$ content for key phases such as amphibole and epidote.

10.2 | Prehnite–pumpellyite to greenschist facies transition

Previous attempts have been made in constructing the phase relations in the prehnite–pumpellyite facies and across the PP-GS transition, including experimental studies (Liou, Kim, & Maruyama, 1983) and theoretical petrogenetic grids (e.g. Frey et al., 1991; Liou et al., 1985; Powell et al., 1993). These studies have resulted in the recognition of a number of subfacies including the prehnite–pumpellyite, pumpellyite–actinolite, prehnite–epidote, and prehnite–actinolite facies.

The NCMASH phase diagram calculated using DS5 (Figure 12a) broadly reproduces these mineral sub-assemblages including the pumpellyite–actinolite (green), prehnite–pumpellyite (red), and prehnite–epidote (yellow) sub-assemblages, and is similar to the petrogenetic grids of Powell et al. (1993) and Liou et al. (1985). The expansion of the chemical system to NCKFMASHTO using the DS6

thermodynamic data set and $a-x$ models, which allows for the incorporation of Fe^{2+} and Fe^{3+} , potentially permits more realistic modelling of the prehnite–pumpellyite to greenschist transition. The phase diagram calculated using DS6 with an $X_{\text{Fe}^{3+}}$ value of 20% (Figure 12d) best replicates the natural sequence of mineral assemblages observed at Flin Flon and within other sequences from the literature, and a simplified summary version of the phase diagram with labelled subfacies fields is presented in Figure 14b. This modelling produces distinct transitional fields including a lower pressure, higher temperature prehnite–epidote field, and a transitional prehnite–actinolite field immediately down-grade of the greenschist facies at low pressure (below ~ 2.3 kbar; Figure 14b).

However, several inconsistencies become apparent when comparing the modelling predictions with observations from Flin Flon and other natural sequences. The first relates to the predicted size of the coexisting prehnite and pumpellyite field (shown in red), which occupies a relatively narrow field in $P-T$ space when modelling with either DS5 (Figure 12a) or DS6 (Figures 12d and 14b). At Flin Flon, the assemblage prehnite–pumpellyite–epidote is widespread and is found considerably down-grade of the PP-GS transition zone, suggesting that it is stable over a range of $P-T$ conditions. There is no evidence for the existence of actinolite or loss of prehnite at very low grades, as predicted by all of the phase diagrams in Figure 12, in Flin Flon or in any other sequence described in the literature. In addition, the following prograde sequence of metamorphic mineral sub-assemblages—prehnite–pumpellyite to pumpellyite–actinolite to greenschist facies assemblages—has been documented in the Otago Schist, New Zealand (Bishop, 1972), which cannot be accommodated in the phase diagrams in Figure 12. This suggests that, in reality, the reaction separating the prehnite–pumpellyite (red) and pumpellyite–actinolite (green) fields has a flatter slope than shown in the phase diagrams in Figure 12, resulting in a larger prehnite–pumpellyite facies field and a more restricted actinolite–pumpellyite field at low pressures.

Perhaps the most important difference is the nature of the PP-GS transition zone. The thermodynamic modelling predicts a PP-GS transition extending across a wide $P-T$ interval characterized by a number of mineral sub-assemblages. The loss of pumpellyite occurs at the lowest grades, resulting in transitional prehnite–epidote and prehnite–actinolite transitional zones and the predicted series of isograds shown in Figure 14b. However, in Flin Flon, the prehnite–pumpellyite zone passes up-grade into a very narrow zone in which actinolite is stable with both prehnite and pumpellyite, and the prehnite-out and pumpellyite-out isograds are coincident within the resolution of the mapping. There is no evidence for the loss of pumpellyite before prehnite and hence there is no evidence for passage through either the predicted prehnite–epidote or prehnite–actinolite subfacies.

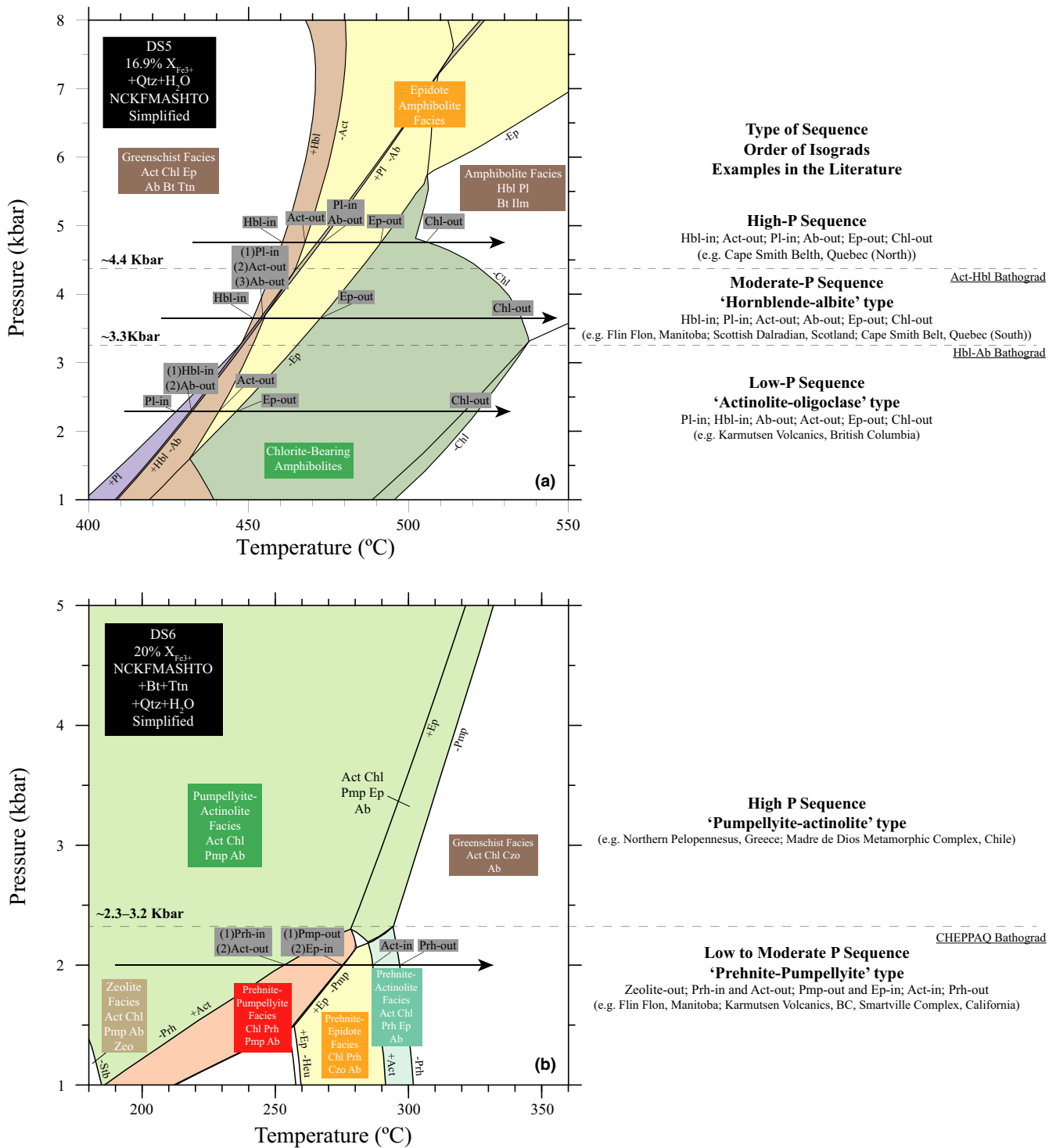


FIGURE 14 Simplified equilibrium P - T phase diagrams demonstrating the main pressure-related metamorphic facies series at greenschist to lower amphibolite facies conditions (a) and prehnite–pumpellyite to greenschist facies conditions (b). (a) Simplified equilibrium P - T phase diagram (NCKFMASHTO) for an average high-Mg basalt with an average calculated Fe^{3+} content (16.9 wt%) at greenschist to lower amphibolite facies conditions calculated using DS5. Three different pressure-related metamorphic series are shown ('actinolite–oligoclase' type; 'hornblende–albite' type; and high-P type), along with the predicted order of isograds and examples from the literature. (b) Simplified equilibrium P - T phase diagram (NCKFMASHTO) for an average high-Mg basalt at prehnite–pumpellyite to lower greenschist facies conditions using DS6 ($X_{Fe^{3+}} = 20\%$). Two different pressure-related metamorphic series (prehnite–pumpellyite type and pumpellyite–actinolite type) are plotted, alongside the predicted order of isograds and literature examples

As discussed previously, similar observations were documented in the Rossland Volcanic sequence (British Columbia, Canada) showing the lack of transitional sub-assemblages (e.g. prehnite–epidote; prehnite–actinolite subfacies) and the rarity of coexisting prehnite or pumpellyite with actinolite (Figure 9). Such observations suggest that, at least in some cases, the nature of the PP–GS transition zone may be quite different from that predicted by the thermodynamic modelling and experimental work (Frey et al., 1991; Liou et al., 1983; Liou et al., 1985; Powell et al., 1993; this study).

Factors that may account for the discrepancies between the above modelling and the natural record include fluid compositional heterogeneity (in particular X_{CO_2}) (Digel & Ghent, 1994), and sensitivity of the mineral assemblages to domain bulk-rock compositions involving variation in parameters such as the Mg/(Mg+Fe) and Fe^{3+}/Fe^{2+} ratios (Day & Springer, 2005; Liou et al., 1985; Springer et al., 1992). The phase equilibria modelling of Digel and Ghent (1994) suggested that prehnite and pumpellyite are only stable in equilibrium with H_2O -rich fluids with X_{CO_2} values of <0.002 . However, in this study, calcite commonly coexists with both prehnite and pumpellyite, including within the same amygdale or phenocryst pseudomorph, suggesting that the prehnite- and pumpellyite-bearing mineral assemblages are not as sensitive to X_{CO_2} fluid content as suggested by Digel and Ghent (1994). Further work is necessary to better characterize the role of fluid composition in controlling mineral assemblages at this grade. The large variation in mineral assemblages and modes within a single thin section supports the idea that small-scale variations in bulk composition, most likely representing inherited igneous or hydrothermal alteration features, results in separate, non-communicating, equilibrium volumes. This may account for different domains dominated by prehnite, pumpellyite or actinolite or all three together. Such compositional heterogeneity cannot be portrayed in phase diagrams calculated for a single bulk composition.

11 | PRESSURE-SENSITIVE FACIES SERIES IN METABASITES

The use of pressure-sensitive metamorphic facies series has been widely recognized as providing useful insights into the tectonic and geodynamic conditions existing during metamorphism (e.g. Carmichael, 1978; Pattison & Tracy, 1991; Pattison & Vogl, 2005; Powell, Carmichael, & Hodgson, 1995). The classic study of Carmichael (1978) demonstrated the existence of a number of pressure-sensitive metamorphic mineral assemblage sequences (bathozones) within metapelite sequences separated by purely pressure-controlled isograds (bathograds) allowing for determination of varying pressure conditions over a wide range of P – T conditions. The analysis of such pressure-sensitive sequences has been

applied to tackle a number of tectonic problems including tracing variable burial depths in orogenic belts (e.g. Bégin, 1992; Powell et al., 1993), determining metamorphic field gradients (e.g. Powell et al., 1995; Todd & Engi, 1997), tracing variable erosion and uplift of metamorphic rocks (e.g. Carmichael, 1978) and testing for post-metamorphic tilting of metamorphic sequences (e.g. Pattison & Vogl, 2005). In this section, we aim to use the detailed examination of the Flin Flon suite and other metabasaltic sequences documented within the literature, combined with the most recent thermodynamic analysis, to provide useful and updated constraints on the P – T conditions of common pressure-sensitive metamorphic facies series in prehnite–pumpellyite to lower amphibolite facies rocks.

11.1 | Greenschist to amphibolite facies transition

The relative order of development of amphibole (actinolite, hornblende) and plagioclase (albite, oligoclase) group minerals in prograde metamorphic sequences has been recognized as a useful indicator of metamorphic pressures within metabasaltic rocks (e.g. Liou et al., 1974; Maruyama et al., 1983; Miyashiro, 1961). Previous studies (e.g. Bégin, 1992; Liou et al., 1974) have shown that the hornblende-in reaction has a steeper slope in P – T space than the oligoclase-producing reaction, resulting in an intersection ('bathograd' in the sense of Bégin, 1992) below which oligoclase develops at lower grade than hornblende, and above which hornblende develops at lower grade than oligoclase (Figure 14a). As described previously, this difference has been observed in prograde metabasaltic sequences from the literature with examples of both hornblende appearing before oligoclase ('hornblende–albite' facies series) and oligoclase before hornblende ('actinolite–oligoclase' type). Despite the recognition of these patterns, the location in P – T space of the intersection between the hornblende-in and oligoclase-in reactions, termed here the hornblende–albite (Hbl–Ab) bathograd, and its sensitivity to bulk compositional variation, is poorly known. Bégin (1992) estimated the position of an invariant point corresponding to the Hbl–Ab bathograd, at 4.8–6 kbar, 460–490°C, using mixed-volatile equilibria calculations.

Figure 14a shows a simplified version of the P – T diagram from Figure 10c, calculated in NCKFMASHTO using DS5, on which are plotted schematic prograde P – T paths (metamorphic field gradients) at different pressures. The lowest pressure metamorphic field gradient ('actinolite–oligoclase type' facies series) is characterized by the appearance of oligoclase before hornblende and predicts the following sequence of reactions (manifested as isograds within the field): Pl-in, Hbl-out, Act-out, Ep-out, Chl-out. Based on Figure 14a, this low pressure, 'actinolite–oligoclase type' facies series

is constrained to pressures below the Hbl-Ab bathograd at less than ~3.3 kbar. The moderate pressure P - T path ('hornblende-albite type' facies series) sequence is characterized by the appearance of hornblende before oligoclase and predicts the following sequence of reactions: Hbl-in, Pl-in, Act-out, Ab-out, Ep-out, Chl-out. This 'actinolite-oligoclase' type sequence is constrained to be above the Hbl-Ab bathograd at greater than ~3.3 kbar. A possible higher pressure P - T path ('actinolite-hornblende type' facies series) is also characterized by the appearance of hornblende before oligoclase, but in contrast to the moderate pressure sequence, actinolite is predicted to be consumed before oligoclase develops. These higher pressure sequences are constrained to be above a second bathograd termed the 'actinolite-hornblende' (Act-Hbl) bathograd at ~4.4 kbar, which occurs at the intersection of the actinolite-out and oligoclase-in reaction lines (Figure 14a). It is important to note that the degree to which actinolite persists above the incoming of hornblende is likely dependent on the kinetically controlled metastable persistence of actinolite going up-grade, as documented in Starr and Pattison (2019a). As a result, the use of this higher pressure facies series and Act-Hbl bathograd as a useful indicator of pressure requires careful analysis of textures.

11.2 | The prehnite-pumpellyite to greenschist facies transition

A potential bathograd separating lower pressure prehnite+chlorite-bearing assemblages and higher pressure pumpellyite+actinolite-bearing assemblages has been suggested based on the interpretation of NCMASH petrogenetic grids (Carmichael, 1991; Powell et al., 1993). This bathograd corresponds to the position of the CHEPPAQ invariant point in NCMASH (Figure 12a), below which samples are predicted to pass through the prehnite-pumpellyite facies and other transitional prehnite-bearing sub-facies, whereas samples at pressures higher than the bathograd pass through the pumpellyite-actinolite facies. There have been a number of estimates for the upper pressure limit of prehnite-pumpellyite facies assemblages, corresponding to this bathograd, based on modelling in NCMASH: ~4 kbar and 320°C (Powell et al., 1993); ~2.7 kbar and 320°C (Liou et al., 1985), and ~2 to 4 kbar and 250–300°C, depending upon the choice of a - x model for prehnite and pumpellyite ('average model' results: 3.2 kbar and 270°C; Frey et al., 1991).

When modelling in NCMASH, using DS5, the CHEPPAQ invariant is constrained to be ~3.2 kbar and 300°C. For a rock undergoing metamorphism at pressures below the 'CHEPPAQ bathograd', the expected mineral assemblage evolves progressively with increasing temperature through the pumpellyite-actinolite, prehnite-pumpellyite, prehnite-epidote, and greenschist facies. The prehnite-pumpellyite

stability field forms a relatively small, thin field that is restricted to ~200 to 280°C and 1.4–3.2 kbar.

If the chemical system is expanded to NCKFMASHTO, the CHEPPAQ invariant point becomes a series of invariant points involving the intersections of reactions involving prehnite, pumpellyite, epidote, and actinolite. In this case, the positioning of the 'CHEPPAQ bathograd' is based on the intersection of the prehnite-out and pumpellyite-out univariant lines, which represents the upper pressure limit for prehnite-bearing assemblages (Figure 14b). The sequence of predicted mineral assemblages is similar to that for modelling in NCMASH, with the addition of a prehnite-actinolite sub-facies (blue field; Figure 14b). The pressure estimate for the 'CHEPPAQ bathograd' varies depending upon the choice of ferric iron content between 2.3 and 2.6 kbar (Figure 12b-d), with increased ferric iron resulting in a lower pressure limit. When modelling with an $X_{Fe^{3+}}$ value of 20% (Figures 12d, 14b), prehnite-pumpellyite facies assemblages are predicted to be stable over a P - T range of ~185–280°C and 1–2.3 kbar, with the transition to greenschist facies conditions at slightly higher temperatures, beginning with the appearance of actinolite at ~290°C and capped by the disappearance of prehnite at ~300°C. As discussed above, rocks of this grade commonly demonstrate local variations in mineral assemblages that likely reflect small equilibration volumes (smaller than a thin section) (see Section 11) and thus care must be taken when correlating the natural observation to phase diagrams representing single bulk compositions.

12 | METAMORPHIC DEVOLATILIZATION WITHIN METABASITES

Metabasites represent the most abundant metamorphic rocks within greenstone belts and thus represent a significant source of metamorphic fluids that may influence geochemical cycling and the formation of ore deposits in these belts. The fluids released during low- to moderate-grade metamorphism of basalts within greenstone belts, particularly across the greenschist-amphibolite facies transition zone, have been proposed as the potential fluid source for orogenic gold deposition (e.g. Elmer et al., 2006; Goldfarb et al., 2005; Goldfarb & Groves, 2015; Powell et al., 1991; Tomkins, 2010, 2013).

The isograd mapping and textural, modal, and compositional data from the Flin Flon sequence suggest that the transition from prehnite-pumpellyite facies to amphibolite facies is characterized by wide zones over which there is little change in the mineral assemblage, mineral modal proportions, or compositions with increasing grade, indicating the absence of progress of continuous reactions within the major facies. Instead, most or all of the change in these metabasites occurs in narrow (~1,000 m), discrete zones of

reaction representing the major facies boundaries, similar to observations from metapelites documented in Pattison, de Capitani, and Gaidies (2011). Correspondingly, it is in these intervals (the prehnite–pumpellyite to greenschist facies and greenschist to amphibolite facies transition zones) where the majority of fluid release occurs.

12.1 | Devolatilization across the greenschist to amphibolite facies transition

The dehydration (i.e. loss of H₂O fluid) and devolatilization (i.e. loss of mixed-volatile fluids) across the greenschist to amphibolite facies transition zone is discussed in detail in a companion paper (Starr & Pattison, 2019b). Thus, only an overview is discussed here, with a focus on the comparison between modelling predictions and observations that relate to metamorphic devolatilization. The modal proportions in rocks of the greenschist and lower amphibolite facies allow for the estimation of mineral-bound water contents at different grades, which can be used in concert with the thermodynamic modelling to assess the amount and intervals of dehydration across the transition.

Figure 15 shows pseudosections calculated using DS5 (Figure 15a) and DS6 (Figure 15b), for the average high-Mg basaltic bulk composition, overlain with contours of the calculated bulk-rock mineral-bound H₂O content. An average of 3.1 wt% H₂O, estimated through combining mineral modes and compositions, for high-Mg basalts within the greenschist facies at Flin Flon and 1.3 wt% H₂O for high-Mg basalts within the lower amphibolite facies (hornblende–oligoclase zone) (Starr & Pattison, 2019b), are similar to the water contents predicted by modelling using the DS5 models (3–3.2 wt% at greenschist facies; 1–1.2 wt% at amphibolite facies), suggesting that the modelling is broadly successful at reproducing the natural observations. A more detailed comparison of the fluid release across the transition zone, however, reveals some differences between the natural observations and the model predictions. The modelling predicts progressive dehydration over a ~50°C interval at moderate pressures beginning with the first appearance of hornblende and continuing until the final breakdown of chlorite (Figures 15a and 13g). By contrast, observations from the Flin Flon sequence suggest that the majority of mineralogical change and dehydration begins only after the first appearance of oligoclase, and occurs over a very narrow interval within the actinolite–hornblende–oligoclase zone, associated with the loss of >75% of the total chlorite content (Figure 6d). The result would have been a large pulse of fluid release over a small spatial and *P–T* window. A detailed assessment of the carbonate and sulphide mineralogy in the Flin Flon sequence, and comparison with the results of *T–XCO₂* modelling, suggests that the fluids generated across the GS–AM transition at

Flin Flon were unlikely to have suitable compositions to be a source fluid for orogenic gold deposit formation (Starr & Pattison, 2019b).

The mineral-bound water contents for greenschist and amphibolite facies rocks and the total amount of dehydration predicted using the DS6 models (Figure 15b) are immaterially different from those produced using DS5. However, using DS6, the fluid release happens over a narrower interval of *P–T* space (Figures 15b, 13h) as a result of a displacement of the chlorite-out line to lower temperatures. In addition, the albite to oligoclase transition plays no role in the dehydration reaction as a result of the displacement of the oligoclase-in reaction to higher temperatures, which is in contrast to natural observations.

12.2 | Devolatilization across the prehnite–pumpellyite to greenschist facies transition

Metamorphic devolatilization across the prehnite–pumpellyite to greenschist facies transition has generally received little attention, in part because of the difficulty in mapping such sequences due to mineral assemblage heterogeneity both at the thin section and outcrop scale. In addition, the limitations in thermodynamic modelling discussed previously have also restricted the capability to model such devolatilization. However, given the potential for minerals such as pumpellyite and prehnite to contain significant amounts of mineral-bound water, dehydration across the transition is likely to be significant.

In contrast to rocks of the greenschist and amphibolite facies, it was not possible to accurately estimate the changes in mineral modal proportions across the PP–GS facies transition in Flin Flon. Mineral modal proportions are highly variable in the natural rocks, implying local bulk compositional domains considerably smaller than the size of a thin section. Thus, establishing parts of the rock or thin section that represented an equilibrium assemblage for a typical bulk composition proved to be impossible.

Despite this, the mapping and petrographic observations, combined with modelling predictions, can still be used to put some bounds on the degree of dehydration across this transition. Figure 15c,d show two phase diagrams, calculated in NCMASH using DS5 (Figure 15c) and in NCKFMASHTO using DS6 (Figure 15d), for the high-Mg basaltic bulk composition. The two phase diagrams are overlain with predicted mineral-bound H₂O contents (in wt% H₂O). In the case of the NCMASH phase diagram calculated using DS5 (Figure 15c), reaction progress and dehydration are predicted to occur at univariant lines, with the majority of dehydration occurring on the actinolite-in line that represents entry into the greenschist facies (1.6–2.0 wt% total H₂O release). However, comparison with the mineral modes and calculated H₂O

of transitional assemblages. In contrast to modelling results, observations from Flin Flon suggest that dehydration occurs as a result of the breakdown of both prehnite and pumpellyite, rather than just prehnite.

Several other observations from the Flin Flon sequence are significant for interpreting the devolatilization across this interval. The first is that, while hard to quantify, there appears to be an apparent decrease in the carbonate modes between the prehnite–pumpellyite facies, where carbonate minerals are common, to the greenschist facies where they are noticeably less abundant. The large number of samples examined suggests that this observation reflects an actual decrease in the proportions of carbonate during the evolution across the PP-GS transition, rather than an artefact of heterogeneous seafloor carbonation. Such a breakdown of carbonate, if indeed coincident with the H₂O release, may result in the production of relatively carbonated fluids. Such fluids may be significant, as the source fluids for orogenic gold formation are generally interpreted to have elevated XCO₂ compositions based on fluid inclusion data and the common appearance of carbonates within gold-hosting vein systems (e.g. Groves, Goldfarb, Gebre-Mariam, Hagemann, & Robert, 1998; Kerrich & Fyfe, 1981). In addition, the loss of carbonate at these grades may restrict the potential for the release of more carbonated fluids at higher grades (Starr & Pattison, 2019b).

A second important observation is the decrease in the remnant igneous mineralogy across the PP-GS transition zone. As this igneous mineralogy (mostly clinopyroxene and plagioclase) is predominantly anhydrous, this conversion to metamorphic mineralogy (e.g. amphibole, epidote, chlorite) requires hydration. This suggests that at least some of the fluid release across this transition zone is consumed in the replacement and hydration of this igneous mineralogy. This fluid is likely important in creating the transition from commonly mixed igneous–metamorphic assemblages in small-scale domainal equilibrium at prehnite–pumpellyite facies to predominantly equilibrated metamorphic assemblages within the lower greenschist facies. As a result, it is unclear what proportion of the fluid released from devolatilization reactions across this transition is lost from the rock package.

13 | CONCLUSIONS

1. The metamorphic grade in the Flin Flon area (Manitoba/Saskatchewan, Canada) ranges from prehnite–pumpellyite to lower amphibolite facies and comprises five regional metamorphic isograds: actinolite-in, prehnite- and pumpellyite-out, hornblende-in, oligoclase-in, and actinolite-out.
2. Across the greenschist–amphibolite facies transition, there are significant increases in the modal amounts of

hornblende and oligoclase coincident with decreases in the modal amounts of actinolite, albite, chlorite, and titanite, but little change in the modal amount of epidote. The transition is characterized first by the appearance of hornblende within the hornblende–actinolite zone, and then by the appearance of oligoclase within the hornblende–actinolite–oligoclase zone, with the majority of reaction progress (marked increase in hornblende and oligoclase, and decrease in chlorite) occurring only after the appearance of oligoclase. Thermodynamic modelling using data set 5 (DS5) of Holland and Powell (1998) and associated *a–x* models is broadly successful in reproducing the sequence of isograds observed over the greenschist–amphibolite facies transition zone at Flin Flon. By contrast, modelling using the data set 6 (DS6) of Holland and Powell (2011) with appropriate *a–x* models predicts mineral assemblages and mineral compositions that are inconsistent with the natural patterns observed at Flin Flon and other similar sequences. This comparison with the natural data set suggests that some modifications to the DS6 plagioclase and amphibole *a–x* models are likely required in order to more accurately model mafic rocks at greenschist and amphibolite facies conditions.

3. Modelling of the prehnite–pumpellyite to greenschist facies transition zone, using either data set 5 (DS5) or data set 6 (DS6), with the appropriate *a–x* models, predicts the existence of a number of mineral subfacies associated with this transition including prehnite–pumpellyite, pumpellyite–actinolite, prehnite–epidote, and prehnite–actinolite subfacies. By contrast, observations from Flin Flon and a similar sequence in Rosslund, British Columbia, suggest no evidence for passage through either a prehnite–epidote or prehnite–actinolite subfacies. Rather, the PP-GS transition occurs over a narrow (<1,000 m) transition zone with the majority of samples typified by mineral assemblages characteristic of either the prehnite–pumpellyite facies or the greenschist facies.
4. In agreement with previous studies, two main pressure-sensitive facies series across the greenschist–amphibolite facies transition zone are predicted on the basis of natural isograd patterns and thermodynamic modelling, with a third pressure series theoretically predicted based on modelling results. The lowest pressure metamorphic facies series ('actinolite–oligoclase type') is characterized by the appearance of oligoclase before hornblende and is constrained to pressures below a Hbl–Ab bathograd at ~3.3 kbar (exact pressure dependent upon the ferric iron content). A moderate pressure facies series ('hornblende–albite type') is characterized by the appearance of hornblende before oligoclase and occurs above the Hbl–Ab bathograd at ~3.3 kbar. A possible

higher pressure facies series ('actinolite–hornblende type') is also characterized by the appearance of oligoclase before hornblende, but actinolite is predicted to be consumed before oligoclase develops. These higher pressure sequences are predicted to occur above an 'actinolite–hornblende' (Act-Hbl) bathograd at ~4.4 kbar, but may be rare in nature because of the metastable persistence of actinolite to higher grades.

5. Within the PP-GS facies transition, a bathograd ('CHEPPAQ bathograd') separating prehnite–pumpellyite-bearing assemblages at low pressures from pumpellyite–actinolite-bearing assemblages at higher pressures is implied by the natural observations and predicted from modelling. When modelling in NCMASH, using DS5, the CHEPPAQ bathograd is constrained to be ~3.2 kbar and 300°C. When the chemical system is expanded to NCKFMASHTO, using DS6, the pressure estimate for the CHEPPAQ bathograd varies between 2.3 and 2.6 kbar, depending upon the choice of ferric iron.
6. Natural observations from Flin Flon and predictions from thermodynamic modelling suggest that the GS-AM transition zone is the site of significant metamorphic devolatilization. Observations from Flin Flon suggest devolatilization (average loss of ~1.8 wt% mineral-bound H₂O from the whole-rock composition) occurs over a very narrow interval within the actinolite–hornblende–oligoclase zone, associated with the loss of >75% of the total chlorite content. This is in contrast to the predictions from thermodynamic modelling, which suggest progressive dehydration of ~2wt% H₂O over a >50°C interval at moderate pressures, beginning with the first appearance of hornblende and continuing until the final breakdown of chlorite.
7. The PP-GS transition is also associated with fluid release from the breakdown of the hydrous minerals, prehnite and pumpellyite. The rarity of transitional assemblages at Flin Flon suggests that the devolatilization interval is very narrow and occurs as a result of the breakdown of both prehnite and pumpellyite. The modelling predicts fluid loss of ~1.0–1.4 wt% H₂O over a ~10°C interval, associated with the breakdown of prehnite and appearance of actinolite in the prehnite–actinolite subfacies. Observations from Flin Flon suggest the fluid released may not be entirely lost from the rock package as there is extensive replacement and hydration of igneous mineralogy coincident with the transition to greenschist facies assemblages.

ACKNOWLEDGEMENTS

We acknowledge R. Marr for assistance with using the electron microprobe and C. Debuhr for support with the scanning electron microscope. We thank E.D. Ghent for helpful discussion and S.G. Digel and E.D. Ghent for allowing us access

to their samples from Flin Flon. We also thank Johann Diener and an anonymous reviewer for their detailed and insightful reviews and Richard White for handling the manuscript. This research was supported by NSERC Discovery Grant 037233 to Pattison.

ORCID

Paul G. Starr  <https://orcid.org/0000-0003-1710-6429>

David R. M. Pattison  <https://orcid.org/0000-0001-5817-6373>

REFERENCES

- Ames, D. E., Galley, A. G., Kjarsgaard, I. M., Tardif, N., & Taylor, B. T. (2016). Hanging-wall vectoring for buried volcanogenic massive sulfide deposits, Paleoproterozoic Flin Flon Mining Camp, Manitoba, Canada. *Economic Geology*, 111(4), 963–1000. <https://doi.org/10.2113/econgeo.111.4.963>
- Ansdell, K. M. (2005). Tectonic evolution of the Manitoba-Saskatchewan segment of the Paleoproterozoic Trans-Hudson Orogen, Canada. *Canadian Journal of Earth Sciences*, 42(4), 741–759. <https://doi.org/10.1139/e05-035>
- Archibald, N. J., Bettenay, L. F., Binns, R. A., Groves, D. I., & Gunthorpe, R. J. (1978). The evolution of Archaean greenstone terrains, Eastern Goldfields Province, Western Australia. *Precambrian Research*, 6(2), 103–131. [https://doi.org/10.1016/0301-9268\(78\)90008-6](https://doi.org/10.1016/0301-9268(78)90008-6)
- Bailes, A. H., & Syme, E. C. (1989). Geology of the Flin Flon-White Lake area. *Manitoba Energy and Mines Geological Services, Geological Report*, 87(1), 313.
- Bégin, N. J. (1992). Contrasting mineral isograd sequences in metabasites of the Cape Smith Belt, northern Québec, Canada: Three new bathograds for mafic rocks. *Journal of Metamorphic Geology*, 10(5), 685–704. <https://doi.org/10.1111/j.1525-1314.1992.tb00115.x>
- Bégin, N. J., & Carmichael, D. M. (1992). Textural and compositional relationships of ca-amphiboles in metabasites of the Cape Smith Belt, Northern Québec: Implications for a miscibility gap at medium pressure. *Journal of Petrology*, 33(6), 1317–1343.
- Bishop, D. G. (1972). Progressive metamorphism from prehnite-pumpellyite to greenschist facies in the dansey pass area, Otago, New Zealand. *Bulletin of the Geological Society of America*, 83(11), 3177–3198. [https://doi.org/10.1130/0016-7606\(1972\)83\[3177:PM-FPTG\]2.0.CO;2](https://doi.org/10.1130/0016-7606(1972)83[3177:PM-FPTG]2.0.CO;2)
- Boyle, A. P. (1986). Metamorphism of basic and pelitic rocks at Sulitjelma, Norway. *Lithos*, 19(2), 113–128. [https://doi.org/10.1016/0024-4937\(86\)90003-4](https://doi.org/10.1016/0024-4937(86)90003-4)
- Brady, J. B. (1974). Coexisting actinolite and hornblende from west-central New Hampshire. *American Mineralogist*, 59, 529–535.
- Carmichael, D. M. (1978). Metamorphic bathozones and bathograds: A measure of the depth of post-metamorphic uplift and erosion on the regional scale. *American Journal of Science*, 278, 769–797. <https://doi.org/10.2475/ajs.278.6.769>
- Carmichael, D. M. (1991). Univariant mixed-volatile reactions: Pressure-temperature phase diagrams and reaction isograds. *Canadian Mineralogist*, 29, 741–754.
- Cho, M., & Liou, J. G. (1987). Prehnite-pumpellyite to greenschist facies transition in the Karmutsen metabasites, Vancouver Island, B.C. *Journal of Petrology*, 28(3), 417–443.
- Coggon, R., & Holland, T. J. B. (2002). Mixing properties of phengitic micas and revised garnet-phengite thermobarometers.

- Journal of Metamorphic Geology*, 20(7), 683–696. <https://doi.org/10.1046/j.1525-1314.2002.00395.x>
- Cooper, A. F. (1972). Progressive metamorphism of metabasic rocks from the Haast Schist Group of Southern New Zealand. *Journal of Petrology*, 13(3), 457–492. <https://doi.org/10.1093/petrology/13.3.457>
- Cooper, A. F., & Lovering, J. F. (1970). Greenschist amphiboles from Haast river, New Zealand. *Contributions to Mineralogy and Petrology*, 27(1), 11–24. <https://doi.org/10.1007/BF00539538>
- Dale, J., Powell, R., White, R. W., Elmer, F. L., & Holland, T. J. B. (2005). A thermodynamic model for Ca–Na clinopyroxenes in Na O–CaO–FeO–MgO–Al O–SiO₂–H₂O–O for petrological calculations. *Journal of Metamorphic Geology*, 23(8), 771–791.
- Day, H. W., & Springer, R. K. (2005). The first appearance of actinolite in the prehnite-pumpellyite facies, Sierra Nevada, California. *Canadian Mineralogist*, 43(1), 89–104. <https://doi.org/10.2113/gscanmin.43.1.89>
- de Capitani, C., & Brown, T. H. (1987). The computation of chemical equilibrium in complex systems containing non-ideal solutions. *Geochimica et Cosmochimica Acta*, 51(10), 2639–2652. [https://doi.org/10.1016/0016-7037\(87\)90145-1](https://doi.org/10.1016/0016-7037(87)90145-1)
- de Capitani, C., & Petrakakis, K. (2010). The computation of equilibrium assemblage diagrams with Theriak/Domino software. *American Mineralogist*, 95(7), 1006–1016. <https://doi.org/10.2138/am.2010.3354>
- Devine, C. A., Gibson, H. L., Bailes, A. H., Maclachlan, K., Gilmore, K., & Galley, A. G. (2002). Stratigraphy of volcanogenic massive sulphide-hosting volcanic and volcanoclastic rocks of the Flin Flon Formation, Flin Flon (NTS 63K12 and 13), Manitoba and Saskatchewan. *Manitoba Geological Society, GS-1*, 9–19.
- DeWolfe, Y. M., Gibson, H. L., & Piercey, S. J. (2009). Petrogenesis of the 1.9 Ga mafic hanging wall sequence to the Flin Flon, Callinan, and Triple 7 massive sulphide deposits, Flin Flon, Manitoba, Canada. *Canadian Journal of Earth Sciences*, 46(7), 509–527.
- Diener, J. F. A., & Powell, R. (2010). Influence of ferric iron on the stability of mineral assemblages. *Journal of Metamorphic Geology*, 28(6), 599–613. <https://doi.org/10.1111/j.1525-1314.2010.00880.x>
- Diener, J. F. A., & Powell, R. (2012). Revised activity-composition models for clinopyroxene and amphibole. *Journal of Metamorphic Geology*, 30(2), 131–142. <https://doi.org/10.1111/j.1525-1314.2011.00959.x>
- Diener, J. F. A., Powell, R., White, R. W., & Holland, T. J. B. (2007). A new thermodynamic model for clino- and orthoamphiboles in the system Na₂O–CaO–FeO–MgO–Al₂O₃–SiO₂–H₂O–O. *Journal of Metamorphic Geology*, 25(6), 631–656.
- Digel, S., & Ghent, E. D. (1994). Fluid-mineral equilibria in prehnite-pumpellyite to greenschist facies metabasites near Flin Flon, Manitoba, Canada: Implications for petrogenetic grids. *Journal of Metamorphic Geology*, 12(4), 467–477. <https://doi.org/10.1111/j.1525-1314.1994.tb00036.x>
- Digel, S. G., & Gordon, T. M. (1995). Phase relations in metabasites and pressure-temperature conditions at the prehnite-pumpellyite to greenschist facies transition, Flin Flon, Manitoba Canada. In P. Schiffman & H. W. Day (Eds.), *Low-grade metamorphism of mafic rocks* (Vol: 296, pp. 67–80). Boulder, CO: Geological Society of America.
- Elmer, F. L., White, R. W., & Powell, R. (2006). Devolatilization of metabasic rocks during greenschist-amphibolite facies metamorphism. *Journal of Metamorphic Geology*, 24(6), 497–513. <https://doi.org/10.1111/j.1525-1314.2006.00650.x>
- Forshaw, J. B., Waters, D. J., Pattison, D. R. M., Palin, R. M., & Gopon, P. (2019). A comparison of observed and thermodynamically predicted phase equilibria and mineral compositions in mafic granulites. *Journal of Metamorphic Geology*, 37, 153–179. <https://doi.org/10.1111/jmg.12454>
- Frey, M., DE Capitani, C., & Liou, J. G. (1991). A new petrogenetic grid for low-grade metabasites. *Journal of Metamorphic Geology*, 9(4), 497–509. <https://doi.org/10.1111/j.1525-1314.1991.tb00542.x>
- Furnes, H., Dilek, Y., & De Wit, M. (2015). Precambrian greenstone sequences represent different ophiolite types. *Gondwana Research*, 27, 649–685. <https://doi.org/10.1016/j.gr.2013.06.004>
- Gale, D., Lucas, S., & Dixon, J. (1999). Structural relations between the polydeformed Flin Flon arc assemblage and Missi Group sedimentary rocks, Flin Flon area, Manitoba and Saskatchewan. *Canadian Journal of Earth Sciences*, 36, 1901–1915. <https://doi.org/10.1139/e99-099>
- Goldfarb, R. J., Baker, T., Dube, B., Groves, D. I., Hart, J. R., & Gosselin, P. (2005). Distribution, character, and genesis of gold deposits in metamorphic terranes. *Economic Geology 100th Anniversary Volume*, 407–450.
- Goldfarb, R. J., & Groves, D. I. (2015). Orogenic gold: Common or evolving fluid and metal sources through time. *Lithos*, 233, 2–26. <https://doi.org/10.1016/j.lithos.2015.07.011>
- Graham, C. M. (1974). Metabasite amphiboles of the Scottish Dalradian. *Contributions to Mineralogy and Petrology*, 47(3), 165–185. <https://doi.org/10.1007/BF00371537>
- Green, E., Holland, T., & Powell, R. (2007). An order-disorder model for omphacitic pyroxenes in the system jadeite-diopside-hedenbergite-acmite, with applications to eclogitic rocks. *American Mineralogist*, 92(7), 1181–1189. <https://doi.org/10.2138/am.2007.2401>
- Green, E. C. R., White, R. W., Diener, J. F. A., Powell, R., Holland, T. J. B., & Palin, R. M. (2016). Activity–composition relations for the calculation of partial melting equilibria in metabasic rocks. *Journal of Metamorphic Geology*, 34(9), 845–869. <https://doi.org/10.1111/jmg.12211>
- Groves, D. I., Goldfarb, R. J., Gebre-Mariam, M., Hagemann, S. G., & Robert, F. (1998). Orogenic gold deposits: A proposed classification in the context of their crustal distribution and relationship to other gold deposit types. *Ore Geology Reviews*, 13(1–5), 7–27. [https://doi.org/10.1016/S0169-1368\(97\)00012-7](https://doi.org/10.1016/S0169-1368(97)00012-7)
- Hawthorne, F. C., Oberti, R., Harlow, G. E., Maresch, W. V., Martin, R. F., Schumacher, J. C., & Welch, M. D. (2012). IMA report: Nomenclature of the amphibole supergroup. *American Mineralogist*, 97(11–12), 2031–2048. <https://doi.org/10.2138/am.2012.4276>
- Hoffman, P. F. (1988). United plates of America, the Birth of a Craton: Early proterozoic assembly of Laurentia. *Annual Review of Earth and Planetary Sciences*, 16, 543–603.
- Holland, T. J. B., Baker, J. M., & Powell, R. (1998). Mixing properties and activity-composition relationships of chlorites in the system MgO–FeO–Al₂O₃–SiO₂–H₂O. *European Journal of Mineralogy*, 10, 395–406. <https://doi.org/10.1127/ejm/10/3/0395>
- Holland, T. J. B., & Powell, R. (1998). An internally consistent thermodynamic data set for phases of petrological interest. *Journal of Metamorphic Geology*, 16(3), 309–343. <https://doi.org/10.1111/j.1525-1314.1998.00140.x>
- Holland, T. J. B., & Powell, R. (2003). Activity-composition relations for phases in petrological calculations: An asymmetric multicomponent formulation. *Contributions to Mineralogy and Petrology*, 145(4), 492–501.

- Holland, T. J. B., & Powell, R. (2011). An improved and extended internally consistent thermodynamic dataset for phases of petrological interest, involving a new equation of state for solids. *Journal of Metamorphic Geology*, 29(3), 333–383. <https://doi.org/10.1111/j.1525-1314.2010.00923.x>
- Katada, M. (1965). Petrography of Ryoke Metamorphic Rocks in Northern Kiso District, Central Japan. *Journal of the Japanese Association of Mineralogists, Petrologists and Economic Geologists*, 53(5), 187–204.
- Kerrick, R., & Fyfe, W. S. (1981). The gold-carbonate association: Source of CO₂, and CO₂ fixation reactions in Archaean lode deposits. *Chemical Geology*, 33, 265–294. [https://doi.org/10.1016/0009-2541\(81\)90104-2](https://doi.org/10.1016/0009-2541(81)90104-2)
- Kremer, P. D., & Simard, R. L. (2007). Geology of the hook lake block, Flin Flon area, Manitoba (part of NTS 63 K/12). Report of Activities 2007, Manitoba Science, Technology, Energy and Mines, Manitoba Geological Survey. pp. 21–32.
- Kretz, R. (1983). Symbols for rock-forming minerals. *American Mineralogist*, 68, 277–279.
- Kuniyoshi, S., & Liou, J. (1976). Contact metamorphism of the Karmutsen Volcanics, Vancouver Island, British Columbia. *Journal of Petrology*, 17, 73–99. <https://doi.org/10.1093/petrology/17.1.73>
- Lafrance, B., Gibson, H. L., Pehrsson, S., Schetselaar, E., DeWolfe, Y. M., & Lewis, D. (2016). Structural reconstruction of the Flin Flon volcanogenic massive sulfide mining district, Saskatchewan and Manitoba, Canada. *Economic Geology*, 111(4), 849–875. <https://doi.org/10.2113/econgeo.111.4.849>
- Leake, B. E., Woolley, A. R., Arps, C. E. S., Birch, W. D., Gilbert, M. C., Grice, J. D., ... Youzhi, G. (1997). Nomenclature of amphiboles; Report of the subcommittee on amphiboles of the international mineralogical association commission on new minerals and mineral names. *European Journal of Mineralogy*, 9(3), 623–651.
- Liou, J. G., Kim, H. S., & Maruyama, S. (1983). Prehnite-epidote equilibria and their petrologic applications. *Journal of Petrology*, 24(4), 321–342. <https://doi.org/10.1093/petrology/24.4.321>
- Liou, J. G., Kuniyoshi, S., & Ito, K. (1974). Experimental studies of the phase relations between greenschist and amphibolite in a basaltic system. *American Journal of Science*, 274, 613–632. <https://doi.org/10.2475/ajs.274.6.613>
- Liou, J. G., Maruyama, S., & Cho, M. (1985). Phase equilibria and mineral parageneses of metabasites in low-grade metamorphism. *Mineralogical Magazine*, 49(352), 321–333.
- Lo Pò, D., & Braga, R. (2014). Influence of ferric iron on phase equilibria in greenschist facies assemblages: The hematite-rich metasedimentary rocks from the Monti Pisani (Northern Apennines). *Journal of Metamorphic Geology*, 32(4), 371–387. <https://doi.org/10.1111/jmg.12076>
- Lucas, S. B., Stern, R. A., Syme, E. C., Reilly, B. A., & Thomas, D. J. (1996). Intraoceanic tectonics and the development of continental crust: 1.92–1.84 Ga evolution of the Flin Flon Belt, Canada. *Geological Society of America Bulletin*, 108(5), 602–629. [https://doi.org/10.1130/0016-7606\(1996\)108<0602:ITATDO>2.3.CO;2](https://doi.org/10.1130/0016-7606(1996)108<0602:ITATDO>2.3.CO;2)
- Maruyama, S., Suzuki, K., & Liou, J. G. (1983). Greenschist-amphibolite transition equilibria at low pressures. *Journal of Petrology*, 24(4), 583–604. <https://doi.org/10.1093/petrology/24.4.583>
- Miyashiro, A. (1961). Evolution of metamorphic belts. *Journal of Petrology*, 2(3), 277–311. <https://doi.org/10.1093/petrology/2.3.277>
- Pattison, D. R. M. (2001). Instability of Al₂SiO₅ “triple-point” assemblages in muscovite+biotite+quartz-bearing metapelites, with implications. *American Mineralogist*, 86, 1414–1422.
- Pattison, D. R. M., de Capitani, C., & Gaidies, F. (2011). Petrological consequences of variations in metamorphic reaction affinity. *Journal of Metamorphic Geology*, 29(9), 953–977. <https://doi.org/10.1111/j.1525-1314.2011.00950.x>
- Pattison, D. R. M., & Tracy, R. J. (1991). Phase equilibria and thermobarometry of metapelites. *Reviews in Mineralogy and Geochemistry*, 26(1), 105–206.
- Pattison, D. R. M., & Vogl, J. J. (2005). Contrasting sequences of metapelitic mineral-assemblages in the aureole of the tilted Nelson Batholith, British Columbia: Implications for phase equilibria and pressure determination in andalusite-sillimanite-type settings. *The Canadian Mineralogist*, 43, 51–88. <https://doi.org/10.2113/gscanmin.43.1.51>
- Powell, R., Will, T. M., & Phillips, G. N. (1991). Metamorphism in Archaean greenstone belts: Calculated fluid compositions and implications for gold mineralization. *Journal of Metamorphic Geology*, 9(2), 141–150. <https://doi.org/10.1111/j.1525-1314.1991.tb00510.x>
- Powell, W. G., Carmichael, D. M., & Hodgson, C. J. (1993). Thermobarometry in a subgreenschist to greenschist transition in metabasites of the Abitibi greenstone belt, Superior Province, Canada. *Journal of Metamorphic Geology*, 11(1), 165–178. <https://doi.org/10.1111/j.1525-1314.1993.tb00138.x>
- Powell, W. G., Carmichael, D. M., & Hodgson, C. J. (1995). Conditions and timing of metamorphism in the southern Abitibi greenstone belt, Quebec. *Canadian Journal of Earth Sciences*, 32, 787–805. <https://doi.org/10.1139/e95-067>
- Rebay, G., Powell, R., & Diener, J. F. A. (2010). Calculated phase equilibria for a MORB composition in a P-T range, 450–650°C and 18–28 kbar: The stability of eclogite. *Journal of Metamorphic Geology*, 28(6), 635–645.
- Schilling, J. G., Zajac, M., Evans, R., Johnston, T., White, W., Devine, J. D., & Kingsley, R. (1983). Petrologic and geochemical variations along the Mid-Atlantic Ridge from 29°N to 73°N. *American Journal of Science*, 283, 510–586.
- Schumacher, J. C. (1997). Appendix 2: The estimation of ferric iron in electron microprobe analysis of amphiboles. *Mineralogical Magazine*, 61(405), 312–321.
- Schumacher, J. C. (2007). Metamorphic amphiboles: Composition and coexistence. *Reviews in Mineralogy and Geochemistry*, 67(1), 359–416. <https://doi.org/10.2138/rmg.2007.67.10>
- Simard, R. L., MacLachlan, K., Gibson, H. L., DeWolfe, Y. M., Devine, C., Kremer, P. D., ... Galley, A. G. (2010). Geology of the Flin Flon area, Manitoba and Saskatchewan (part of NTS 63K12, 13). Manitoba Innovation, Energy and Mines, Manitoba Geological Survey, Geoscientific Map MAP 2010–1.
- Spear, F. S., & Cheney, J. T. (1989). A petrogenetic grid for pelitic schists in the system SiO₂-Al₂O₃-FeO-MgO-K₂O-H₂O. *Contributions to Mineralogy & Petrology*, 101, 149–164. <https://doi.org/10.1007/BF00375302>
- Springer, R. K., Day, H. W., & Beiersdorfer, R. E. (1992). Prehnite-pumpellyite to greenschist facies transition, Smartville Complex, near Auburn, California. *Journal of Metamorphic Geology*, 10(2), 147–170. <https://doi.org/10.1111/j.1525-1314.1992.tb00076.x>
- Starr, P. G., & Pattison, D. R. M. (2019a). Equilibrium and disequilibrium processes across the greenschist – Amphibolite transition zone in metabasites. *Contributions to Mineralogy and Petrology*, 174(2), 1–18. <https://doi.org/10.1007/s00410-019-1553-y>
- Starr, P. G., & Pattison, D. R. M. (2019b). Metamorphic devolatilization of basalts across the greenschist-amphibolite facies transition zone: Insights from isograd mapping, petrography and thermodynamic

- modelling. *Lithos*, 342–343, 295–314. <https://doi.org/10.1016/j.lithos.2019.05.020>
- Stauffer, M. R. (1984). Manikewan: An early proterozoic ocean in central Canada, its igneous history and orogenic closure. *Precambrian Research*, 25(1–3), 257–281. [https://doi.org/10.1016/0301-9268\(84\)90036-6](https://doi.org/10.1016/0301-9268(84)90036-6)
- Syme, E. C., Lucas, S. B., Bailes, A. H., & Stern, R. A. (1999). Contrasting arc and MORB-like assemblages in the Paleoproterozoic Flin Flon Belt, Manitoba, and the role of intra-arc extension in localizing volcanic-hosted massive sulphide deposits. *Canadian Journal of Earth Sciences*, 36(11), 1767–1788. <https://doi.org/10.1139/e98-084>
- Terabayashi, M. (1993). Compositional evolution in Ca-amphibole in the Karmutsen metabasites, Vancouver Island, British Columbia, Canada. *Journal of Metamorphic Geology*, 11(5), 677–690. <https://doi.org/10.1111/j.1525-1314.1993.tb00180.x>
- Todd, C. S., & Engi, M. (1997). Metamorphic field gradients in the Central Alps. *Journal of Metamorphic Geology*, 15, 513–530. <https://doi.org/10.1111/j.1525-1314.1997.00038.x>
- Tomkins, A. G. (2010). Windows of metamorphic sulfur liberation in the crust: Implications for gold deposit genesis. *Geochimica et Cosmochimica Acta*, 74(11), 3246–3259.
- Tomkins, A. G. (2013). On the source of orogenic gold. *Geology*, 41(12), 1255–1256. <https://doi.org/10.1130/focus122013.1>
- White, R. W., Pomroy, N. E., & Powell, R. (2005). An in situ metatexite-diatexite transition in upper amphibolite facies rocks from Broken Hill, Australia. *Journal of Metamorphic Geology*, 23(7), 579–602. <https://doi.org/10.1111/j.1525-1314.2005.00597.x>
- White, R. W., Powell, R., & Clarke, G. L. (2002). The interpretation of reaction textures in Fe-rich metapelitic granulites of the Musgrave Block, Central Australia: Constraints from mineral equilibria calculations in the system. *Journal of Metamorphic Geology*, 20(1), 41–55.
- White, R. W., Powell, R., & Holland, T. J. B. (2007). Progress relating to calculation of partial melting equilibria for metapelites. *Journal of Metamorphic Geology*, 25(5), 511–527. <https://doi.org/10.1111/j.1525-1314.2007.00711.x>
- White, R. W., Powell, R., Holland, T. J. B., Johnson, T. E., & Green, E. C. R. (2014). New mineral activity-composition relations for thermodynamic calculations in metapelitic systems. *Journal of Metamorphic Geology*, 32, 261–286. <https://doi.org/10.1111/jmg.12071>
- White, R. W., Powell, R., Holland, T. J. B., & Worley, B. (2000). The effect of TiO₂ and Fe₂O₃ on metapelitic assemblages at greenschist and amphibolite facies conditions: Mineral equilibria calculations in the system K₂O-FeO-MgO-Al₂O₃-SiO₂-H₂O-TiO₂-Fe₂O₃. *Journal of Metamorphic Geology*, 18, 497–511. <https://doi.org/10.1046/j.1525-1314.2000.00269.x>
- Zane, A., & Weiss, Z. (1998). A procedure for classifying rock-forming chlorites based on microprobe data. *Rendiconti Lincei*, 9, 51–56.

SUPPORTING INFORMATION

Additional supporting information may be found online in the Supporting Information section.

Figure S1. Thermodynamically calculated equilibrium *P–T* phase diagrams (NCKFMASHTO) calculated for the average high-Mg basalt bulk composition, using data set 6 (DS6) of Holland and Powell (2011), with different modifications of the Green et al., (2016) amphibole model.

Table S1. Modal data for the Flin Flon volcanics.

Table S2. Selected amphibole data for the Flin Flon volcanics.

Table S3. Selection of plagioclase data for the Flin Flon suite.

Table S4. Epidote compositional data for the Flin Flon suite.

Table S5. Selection of chlorite data from the Flin Flon suites.

Table S6. Complete list of bulk compositions (calculated from compositions and modes; XRF).

Table S7. Average bulk compositions (mol%) of the main compositions groups (high-Mg, high-Ca and high-Na basalts) used for modelling.

How to cite this article: Starr PG, Pattison DRM, Ames DE. Mineral assemblages and phase equilibria of metabasites from the prehnite–pumpellyite to amphibolite facies, with the Flin Flon Greenstone Belt (Manitoba) as a type example. *J Metamorph Geol*. 2019;00:1–32. <https://doi.org/10.1111/jmg.12513>